MINISTERE DE L'ENSEIGNEMENT SUPERIEUR
ET DE LA RECHERCHE SCIENTIFIQUE

Felix Houphouët-Boigny University

UNITE DE FORMATION ET DE RECHERCHE
SCIENCES DES STRUCTURES DE LA
MATIERE ET DE TECHNOLOGIE

RÉPUBLIQUE DE CÔTE D'IVOIRE
UNION - DISCIPLINE - TRAVAIL

N°: 840

INTERNATIONAL MASTER PROGRAM

IN RENEWABLE ENERGY AND GREEN HYDROGEN

SPECIALITY: PRODUCTION AND TECHNOLOGY OF GREEN HYDROGEN

MASTER THESIS

TOPIC

Synthesis and Characterization of Amine-Modified Carbon Nanofibers for Direct Air Capture of CO_2

Presented on September 26, 2025 by:

Saadatou SEYNI HAROUNA

Jury:

Dr. (MC) ZORO Georgina Emma	**President**
Prof. ESSI Marc Marie-Maurice Mélèdge	**Examiner**
Dr. KOFFI Aka Stéphane	**Supervisor**
Prof. Rüdiger Eichel	**Co-Supervisor**
Dr. Victor Selmert	**Co-Supervisor**
Carl Jung	**Co-Supervisor**

Academic year: 2024-2025

DEDICATION

“To my late father, who would have been proud of this achievement. May The Almighty grant him peace and the highest place in Jannah.

To my beloved mother, whose prayers, sacrifices, and love have served as the foundation of my determination

To my brothers and sisters, thank you for your constant affection and for being my companions in both joy and challenge.

To my beloved husband, whose love, patience, and constant support have been a pillar of strength in my life; to my parents-in-law, whose warm acceptance, prayers and moral support gave me the courage to persevere

This work is lovingly dedicated to you.”

ACKNOWLEDGMENTS

First and foremost, I would like to thank the Almighty for granting me health, strength, and perseverance throughout this journey.

I am thankful to the German Federal Ministry of Research, Technology and Space (BMFTR) for its financial support through the West African Science Service Centre on Climate Change and Adapted Land Uses (WASCAL) International Master Program in Energy and Green Hydrogen. This study would not have been possible without it.

I extend my appreciation to the President of the University Félix Houphouët-Boigny of Abidjan the Rector of University of Lome, the Rector of Abdou Moumouni University in Niamey for making it possible for me to pursue my academic program across these institutions. I also extend my gratitude to Prof. Dr. Rüdiger-A. Eichel, Director of the IET-1 at Forschungszentrum Jülich, for hosting me during my internship in Germany.

Many thanks to Prof. Rabani Adamou, Director of WASCAL Niger, Prof. Kouassi Edouard, Director of WASCAL Côte d'Ivoire, Dr. FASSINOU Ferdinand, the H_2 program coordinator, and Prof. Soro, the scientific coordinator for their support and leadership. I am grateful to my major supervisor. Dr. KOFFI Aka Stephane, for his invaluable guidance and support throughout this work.

I am very thankful to Dr. (MC) ZORO Georgina Emma, President of the Jury, and Prof. ESSI Marc Marie-Maurice Mélèdge, Examiner, for their expertise and constructive feedback, which have contributed to the improvement of this thesis.

I extend my profound thanks to my daily supervisors, Dr. Victor Selmert and Carl Jung, for their continuous encouragement, patience, and guidance during this journey.

I also extend my thanks to Dr. Ansgar Kretzschmar for his insightful feedback and the Adsorption Team, for creating a very supportive research environment.

ABSTRACT

This work investigates the development and evaluation of aminosilane-functionalized carbon nanofibers as adsorbents for Direct Air Capture. The study focused on the impact of surface modification and textural tailoring on CO_2 adsorption performance under ultradilute conditions (~400 ppm), ambient temperature, and in the presence of atmospheric humidity.

A series of modifications was applied to electrospun PAN fibers, such as stabilization, carbonization, oxidation with $H_2SO_4/KMnO_4$, KOH activation, and silanization with (3-aminopropyl)trimethoxysilane (APTMS). Energy-Dispersive X-ray Spectroscopy (EDX), BET surface area measurements, pore size distribution, Thermogravimetric Analysis (TGA), and Scanning Electron Microscopy (SEM) were used to analyze the structural, morphological, and surface chemical properties of the fibers. H_2O and CO_2 adsorption isotherms, were performed to evaluate performance under conditions that are similar to direct air capture.

The unmodified and oxidized carbon nanofibers showed limited microporosity and low BET surface areas of 7.8 and 77.6 $m^2\ g^{-1}$, respectively, resulting in negligible CO_2 uptake (< 0.1 mmol g^{-1} at 400 ppm CO_2). The introduction of oxygen-containing groups during oxidation was verified by TGA, which resulted in an increase in the surface functionality. KOH activation expanded microporosity, raising the BET surface area to 436.9 $m^2\ g^{-1}$ and micropore volume to 0.239 $cm^3\ g^{-1}$. This resulted in a physisorptive CO_2 capacity of approximately 0.45 mmol g^{-1} at 400 ppm. The greatest enhancement was achieved by APTMS silanization, which grafted primary amines onto carbon nanofiber surfaces, yielding a surface area of 58.9 $m^2\ g^{-1}$ and CO_2 uptake exceeding 0.7 mmol g^{-1} under DAC-relevant conditions.

Overall, this work shows that the combination of KOH activation and APTMS functionalization creates CNFs with complementary improvements in porosity and surface chemistry, enabling enhanced CO_2 capture performance under DAC scenarios. The results show that optimizing functionalization protocols such as coating time, reagent quantities, and grafting conditions, is essential to enhance adsorbents performance.

Keywords: Direct Air Capture, Carbon nanofibers, CO_2 adsorption, Aminosilane functionalization, KOH activation

RESUMÉ

Ce travail porte sur le développement et l'évaluation de nanofibres de carbone fonctionnalisées par un aminosilane comme adsorbants pour la capture directe du CO_2 dans l'air (DAC). L'étude a porté sur l'impact de la modification de surface et de l'ajustement textural sur les performances d'adsorption du CO_2 dans des conditions ultradiluées (~400 ppm), à température ambiante et en présence d'humidité atmosphérique.

Les fibres de polyacrylonitrile (PAN) ont subi une séquence de traitements comprenant une carbonisation, une oxydation realisée par $H_2SO_4/KMnO_4$, une activation par KOH et une silanisation effectuée par le (3-aminopropyl)triméthoxysilane (APTMS). Les propriétés structurales, morphologiques, chimiques de surface ont été analysées par microscopie électronique à balayage (SEM) couplée à l'EDX, par des mesures de surface spécifiques selon la méthode BET, par l'analyse de la distribution de tailles de pores et par analyse thermogravimétrique (TGA). Les performances d'adsorption ont été évaluées par des isothermes de CO_2 et de H_2O ainsi que par des tests dynamiques de percée, réalisés dans des conditions représentatives de la DAC.

Les nanofibres non modifiées et oxydées ont présenté une microporosité limitée et de faibles surfaces spécifiques (7,8 et 77,6 $m^2\ g^{-1}$ respectivement), conduisant à une adsorption négligeable du CO_2 (< 0,1 mmol g^{-1} à 1 bar, 400 ppm). L'oxydation, confirmée par TGA, a cependant permis d'introduire des groupements oxygénés améliorant la fonctionnalité de surface. L'activation par KOH a considérablement augmenté la microporosité avec une surface spécifique de 436,9 $m^2\ g^{-1}$ et un volume microporeux de 0,239 $cm^3\ g^{-1}$, et une capacité physisorptive de 0,45 mmol g^{-1} à 400 ppm. La modification par APTMS a apporté l'amélioration la plus importante : le greffage d'amines primaires a permis d'obtenir une surface spécifique de 58,9 $m^2\ g^{-1}$ et une capacité d'adsorption de plus de 0,7 mmol g^{-1} dans des conditions de DAC.

Globalement, ces résultats mettent en évidence que l'association de l'activation par KOH et de la fonctionnalisation par APTMS octroie aux nanofibres de carbone des améliorations complémentaires en termes de porosité et de propriétés chimiques des surfaces, augmentant ainsi leur efficacité pour la capture du CO_2 atmosphérique. L'optimisation des paramètres des protocoles de fonctionnalisation, notamment la durée de la réaction, la quantité de réactif et les conditions de greffage se révèle cruciale pour optimiser les performances de ces adsorbants.

Mots-clés : Nanofibres de carbone ; Activation par KOH ; Fonctionnalisation de surface ; APTMS ; Adsorption de CO_2

TABLE OF CONTENTS

LIST OF ABBREVIATIONS AND ACRONYMS

APTMS	: (3-aminopropyl)trimethoxysilane
BET	: Brunauer-Emmett-Teller
BMFTR	: Federal Ministry of Research, Technology and Space
BTC	: Breakthrough Column Curve
CNF	: Carbon Nanofibers
DAC	: Direct Air Capture
DVS	: Dynamic Vapor Sorption
EDX	: Energy-Dispersive X-ray Spectroscopy
IPCC	: Intergovernmental Panel on Climate Change
IUPAC	: International Union of Pure and Applied Chemistry
MOFs	: Metal-Organic Frameworks
NETs	: Negative Emissions Technologies
PAN	: Polyacrylonitrile
PEI	: Polyethylenimine
Ppm	: Parts Per Million
RH	: Relative Humidity
SEM	: Scanning Electron Microscopy
TGA	: Thermogravimetric Analysis
VP OC	: Versuchsprodukt Organic Compound

LIST OF FIGURES

LIST OF TABLES

GENERAL INTRODUCTION

GENERAL INTRODUCTION

The extensive use of fossil fuels, rapid industrial growth, intensive agricultural practices, systematic deforestation, and human-induced carbon dioxide (CO_2) emissions have increased since the Industrial Revolution. (Yagmur Goren et al., 2024) The atmospheric CO_2 level reached 412 ppm by 2020, up from 280 ppm in 1750, the greatest level in almost two million years.(Yagmur Goren et al., 2024) Human activities, especially fossil fuel use and deforestation, have raised atmospheric CO_2 levels to about 430 ppm in 2025. This increase has caused the global surface temperature to rise by approximately 1.3 ^{o}C above the pre-industrial levels by 2025, driving significant climate change impacts. (Hansen et al., n.d.; Sodiq et al., 2023) According to the Intergovernmental Panel on Climate Change (IPCC), rising global energy consumption could cause annual CO_2 emissions to reach 52-58 (Gt) by 2030 if nothing is done. (Shi et al., 2020)

Among the growing strategies to address climate change, technologies that remove CO_2 from the atmosphere are gaining considerable attention. These are often referred to as Negative Emission Technologies (NETs), and they include bio-based approaches such as afforestation and reforestation, bioenergy with carbon capture and storage (BECCS), soil carbon sequestration, and ocean-based methods, as well as technology-driven methods summarized in the term Direct Air Capture (DAC). There is considerable interest in technologies that directly remove CO_2 from the atmosphere, as these remove considerably more CO_2 in the same time span and require less space than biomass-based approaches. It can potentially reduce diffuse and legacy emissions that point-source capture cannot address.

A combination of technological and financial obstacles prevents DAC from being deployed at large scales. The main obstacle is the naturally low atmospheric concentration of CO_2 (~0.04%), which has major kinetic and thermodynamic disadvantages for sorbent-based capture techniques. This calls for the urgent search for novel sorbent materials with high CO_2 selectivity, quick kinetics, resistance to ambient humidity, low regeneration energy, and long-term performance over multiple cycles.

Electrospun carbon nanofibers (CNFs), especially those made from polyacrylonitrile (PAN), are a potential base for advanced direct air capture adsorbents. These nanofibers have a large surface area, an open networked structure and numerous nitrogen-containing functional groups that can be tailored to improve CO_2 capture.

According to Kretzschmar et al. (2020), carbons offer a unique set of advantages over conventional materials like zeolites and metal-organic frameworks (MOFs): they are abundant, affordable, reasonably simple to synthesize, and less sensitive to impurities like water. However, even the best unaltered CNFs have limitations, particularly in practical, humid settings and during the repetitive cycles that are typical of DAC operations.

Aminosilane functionalization is a workable way to get around these restrictions. This modification can significantly improve CO_2 adsorption at low concentrations, selectivity, and stability by adding primary amine groups and a hydrophobic siloxane scaffold to the CNF surface.

The main objective of this thesis is to synthesize and analyze aminosilane-modified carbon nanofibers. The goal is to assess their capacity to capture CO_2 in conditions that are comparable to direct air capture and to compare their performance to benchmark sorbents, such as Lewatit VP OC 1065 and PEI-impregnated CNFs. In order to investigate the impact of surface chemistry and structure on adsorption behavior, analysis techniques such as SEM, TGA, and adsorption measurements are implemented.

The adsorption of CO_2 is expected to be improved by the introduction of amine functionalities. Pretreatment conditions are expected to influence the equilibrium between amine loading and the prevention of accessible porosity, which will determine the extent of this enhancement.

This thesis is organized into three main chapters: Chapter 1 provides a literature review; Chapter 2 details the materials and methods used for synthesizing and characterizing aminosilane-modified carbon nanofibers; Chapter 3 presents and discusses the experimental results including adsorption performance and material analysis. This work concludes with a final section offering conclusions and perspectives for future DAC sorbent development.

CHAPTER 1:
LITERATURE REVIEW

CHAPTER 1- Literature Review

In this chapter, we will explore direct air capture (DAC) concepts, including adsorption and CO_2 removal, and review current technologies and their advantages and disadvantages. It will also highlight the potential of carbon nanofibers as advanced sorbents, discuss surface modification techniques, and compare benchmark sorbents.

1.1 General Principles of Adsorption

1.1.1 Definition

Adsorption is a surface phenomenon. It involves the adhesion of atoms, ions, or molecules from a fluid, gas or liquid onto the surface of a solid or liquid interface. When a substance comes into contact with a surface, called the adsorbent, it accumulates only on the surface or within the pores, rather than being fully integrated into the bulk of the material. This surface accumulation is typically driven by the physical forces, such as Van der Waals interactions or by the formation of chemical bonds.

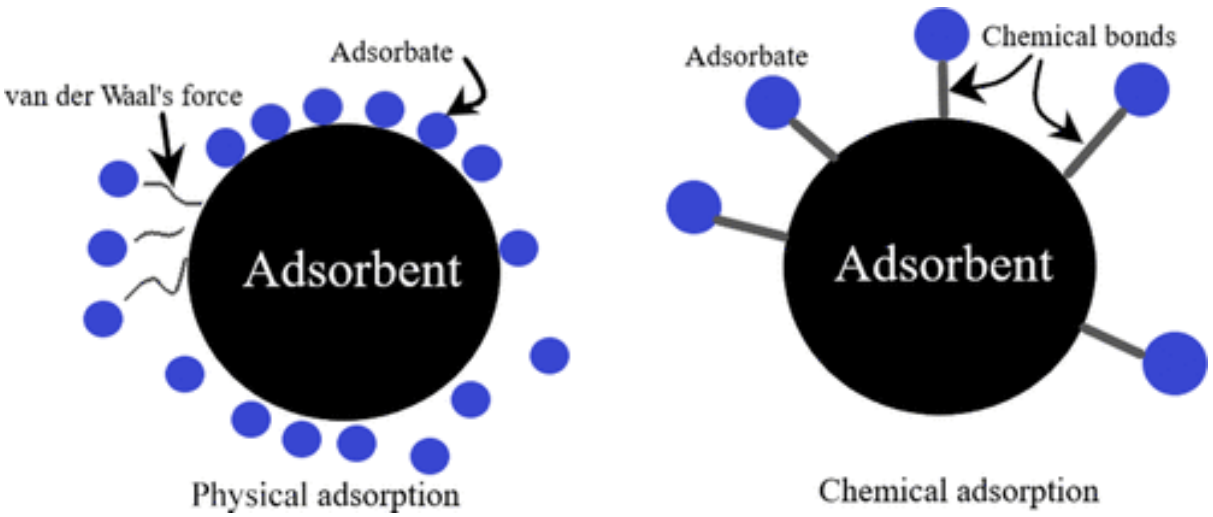

Figure 1: Physical and chemical types of adsorption. (Moosavi et al., 2020)

In contrast, absorption is a bulk phenomenon, where the absorbate penetrates the entire volume of the material. In summary, adsorption adds molecules to the surface, while absorption brings them into the material.

1.1.2 Types of adsorption

1.1.2.1 Physical adsorption

Physical adsorption or physisorption involves weak, non-specific interaction, primarily Van der Waals forces between the adsorbate and the adsorbent surface. The process is usually reversible, occurs at low temperature and increases with decreasing temperature. There is no significant change in the chemical identity of the adsorbate and the adsorbent. This process does not require significant energy input.

1.1.2.2 Chemical adsorption

Chemical adsorption, or chemisorption, is based on the formation of chemical bonds, such as ionic or covalent, between the adsorbate and specific sites on the adsorbent surface. In this type of adsorption, the interactions are stronger and often specific to certain chemicals, groups or surface sites. It usually involves just a single molecular layer (monolayer) because once a site is occupied, no further adsorption can occur at the same spot. It requires activation energy. The reaction is often irreversible or requires significant energy to reverse.

1.1.3 Adsorption isotherms

Adsorption isotherms are important for figuring out how gases like CO_2 behave when they came into contact with solid surfaces at equilibrium conditions. They explain how the quantity of gas that a material can store relates to the gas pressure (for gas) or concentration (for liquids) at a fixed temperature.

The Langmuir model suggests a homogeneous surface with adsorption sites, demonstrating monolayer adsorption without molecular interactions. It is helpful for chemisorption and materials where a single layer of CO_2 creates active sites.

The Freundlich model is empirical and assumes a heterogeneous surface with adsorption sites of varying energies. It is particularly useful for describing physisorption on porous materials such as activated carbon or metal-organic frameworks.(Zhang et al., 2024)

The Brunauer-Emmett-Teller (BET) isotherm extends the Langmuir model to account for multilayer adsorption and is commonly used to estimate the specific surface area of porous materials. Although it is not typically used to model CO_2 adsorption directly, BET analysis is critical during material characterisation.

The International Union of Pure and Applied Chemistry (IUPAC) classifies six adsorption isotherms (Types I to VI) based on surface and pore characteristics of adsorbent materials, which are shown in Figure 2.

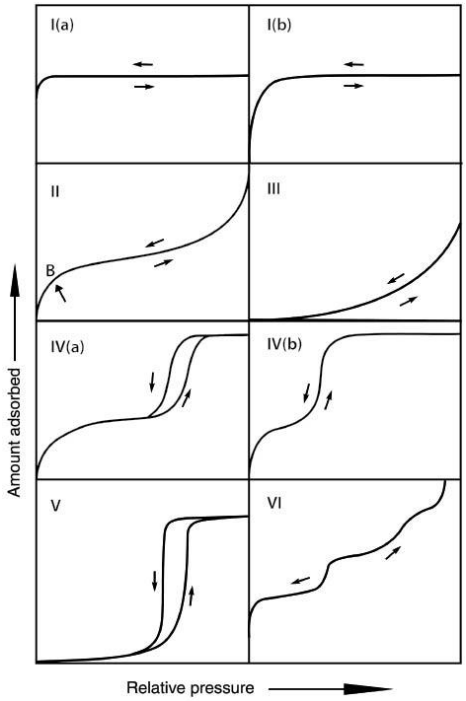

Figure 2: Classification of physisorption isotherms. (Thommes et al., 2015a)

Type I isotherms are reversible in adsorption processes. Type I(a) is for microporous solids with small exterior surfaces, while Type I(b) is for materials with a wider range of pore sizes. Type II isotherms happen when gases are physically adsorbed on adsorbents that are not porous or have large pores. (Thommes et al., 2015a). Type III isotherms do not have a Point B, and the interactions between the adsorbent and the adsorbate are weak. Point B indicates the onset of multilayer adsorption on the adsorbent surface, marking the transition from monolayer to multilayer. Mesoporous adsorbents create Type IV isotherms. When the pore width is in the range of mesopores, capillary condensation and hysteresis happen. Type V isotherms resemble Type III isotherms at low p/p0 ranges, but exhibit hysteresis. Type VI isotherms display how adsorption happens layer by layer on smooth, nonporous surfaces.(Thommes et al., 2015a)

1.1.4 Adsorption hysteresis

Adsorption hysteresis is a common phenomenon observed when measuring how much gas is adsorbed and then desorbed from a porous material as the pressure is cycled (Figure 3). Instead of following the same path in both directions, the adsorption and desorption branches form a

loop, meaning the amount of gas remaining on the material at a given pressure differs depending on whether the pressure is increasing or decreasing. (Thommes et al., 2015b)

Hysteresis is usually connected to capillary condensation in mesopores that are 2 to 50 nm wide. During adsorption, the condensate inside the pores acts like liquid and forms at lower relative pressures than predicted. On the other hand, desorption needs a lot less pressure to happen. This difference makes the loop shape, which shows that evaporation happens after condensation because of the confinement effect.

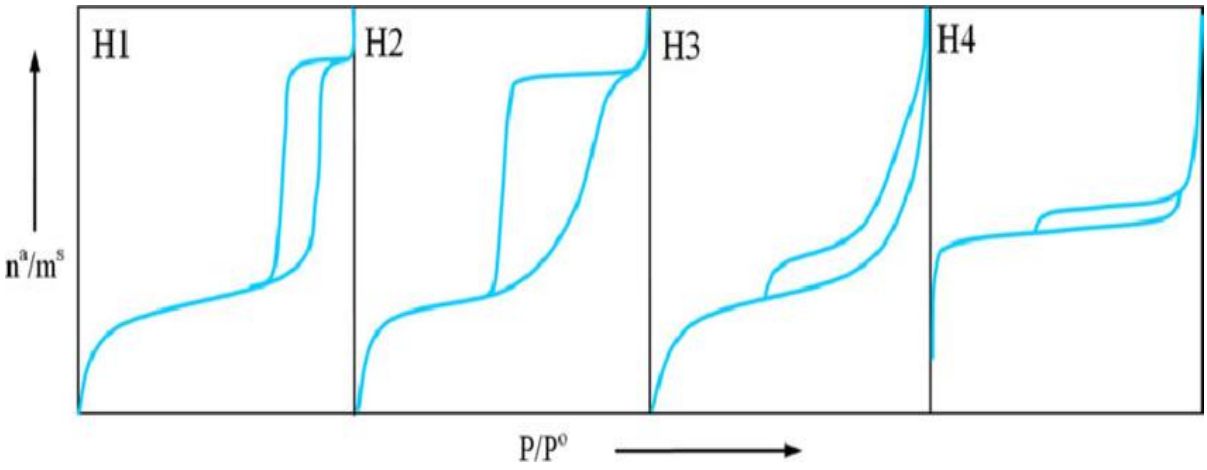

Figure 3: The four hysteresis loops of adsorption isotherms by IUPAC classification(Chang et al., 2009)

1.1.5 Heat of adsorption

The heat of adsorption describes the energy released when a gas molecule interacts with the surface of an adsorbent. It reflects the strength of interactions between the adsorbate and the surface and provides crucial insights into the nature of adsorption. In simple terms, it is a measure of how strongly a molecule like CO_2 is attracted to a material like CNFs.

In physisorption these interactions are dominated by van der Waals forces or electrostatic attractions, resulting in relatively low heats of adsorption typically ranging between -10 to -40 kJ mol^{-1}. By contrast, chemisorption involves the formation of stronger, often covalent-like bonds, such as the reaction of CO_2 with amine groups, resulting in significantly higher values, generally in the range of -60 to -100 kJ mol^{-1} (Gunawardene et al., 2022; Raganati et al., 2021)

In porous carbon and carbon nanofibers, the heat of adsorption typically begins around -20 to 30 kJ mol^{-1} at low CO_2 coverage, gradually decreasing as the most energetically favorable sites are occupied.(Shi et al., 2020)

In contrast, amine functionalized sorbents exhibit substantially higher heats of adsorption often exceeding 60 kJ mol^{-1} due to the formation of carbamate or bicarbonate species, highlighting the strong chemisorption nature of the interaction.(Gunawardene et al., 2022)

This increase in binding strength enhances CO_2 capture capacity and selectivity and raises the energy needed for adsorbent regeneration.(Raganati et al., 2021)

The heat of adsorption serves as an essential descriptor for evaluating adsorbents in DAC application.

1.2 DAC Technologies

1.2.1 Overview of Direct Air Capture (DAC)

As the need for negative emission technologies (NETs) has increased, carbon capture systems have changed to target CO_2 at different levels of emissions and concentrations. Klaus Lackner first talked about DAC in the 1990s, and since then it has been more popular in both academic and industrial research. (Shi et al., 2020) In sectors such as aviation and chemical manufacturing, where decarbonization options are limited, ongoing research aims to develop advanced, durable, and efficient sorbents to enable direct air capture (DAC) to be both technically viable and practical. (Fuss et al., 2018; Yagmur Goren et al., 2024). DAC is a more flexible and location-independent way to remove CO_2. It can work in both cities and isolated areas without needing concentrated emission streams.

According to the International Energy Agency (IEA), there are now twenty-seven DAC plants operating worldwide that capture more than 0.01 Mt of CO_2 per year. A plan for a minimum of 130 large-scale DAC plants, each exceeding 1000 tons of CO_2 annually, is now at various stages of development.

The main function or role of a DAC system (Figure 4) is to bring large amounts of air into contact with a specially engineered material, either a solid sorbent or a liquid solvent, which binds CO_2 molecules selectively. The collected CO_2 is released in a concentrated form when the material is saturated, usually by heating it or applying a vacuum. The purified CO_2 can be compressed and sent underground for long-term storage or employed in the production of chemicals, construction materials, or synthetic fuels like methanol.

The success of DAC systems depends on the creation of improved adsorbent materials that have high surface areas, adjustable pore shapes, and strong chemical and thermal stability. These characteristics are necessary to guarantee enough adsorption capacity and operational durability, especially considering that the partial pressure of CO_2 in the air is low (about 400 ppm). (Shi et al., 2020)

Figure 4: Direct Air Capture (DAC) Device. (*SOLARIFY*, n.d., 2025)

1.2.2 Current materials and their limitations

The first version of DAC systems mostly used potassium hydroxide (KOH) or sodium hydroxide (NaOH) dissolved in water or amine-based liquid solevnt to chemically collect CO_2. These systems work well to remove CO_2, but they have a lot of problems, such as using a lot of energy during regeneration, being corrosive, breaking down through oxidation and being volatile. (Shi et al., 2020)

These issues have led to the development of solid adsorbents, which are expected to be more stable, less corrosive, and easier to renew in mild environments. There are three major ways that solid sorbents interact with CO_2: physiosorption, chemisorption and a mix of the two. Chemisorptive compounds such as metal oxides, hydroxides and alkaline salts have strong, usually covalent bonds with carbon dioxide. Because of this, they can hold a lot of CO_2. But since these systems have such strong bonds, they need high regeneration temperatures, which usually involves calcination or other procedures that use a lot of energy, which makes them less energy-efficient.(Shi et al., 2020)

On the other hand, physisorptive materials like activated carbons and porous polymers interact with CO_2 less strongly through Van der Waals forces, which makes regeneration happen quicker at lower temperatures. However, they are not very good at DAC since they do not have a lot of selectivity, and their capacity is poor at the low partial pressures seen in ambient air. (McQueen et al., 2021)

Moisture-swing sorbents are a potential compromise because they change how much CO_2 they attract when water vapor is present. In general, these materials hold onto CO_2 when it is dry and let it go when it is humid, so they do not need to be heated up to get it back. Nanostructured materials are also becoming more popular in the DAC field. Their high surface-to-volume ratios make it easier for CO_2 to get to and adsorb to them.

Amine-functionalized materials are one of the most common types of solid sorbents because they may change how they chemisorb. They are generally attached to porous surfaces like silica, alumina, or mesoporous polymers. However, they are sensitive to moisture, which can compete with CO_2 for binding sites and reduce efficiency, especially in humid climates.

Metal-organic frameworks (MOFs) have attracted considerable attention due to their flexible pore structures and chemical adaptability. Recent advances, such as AI-driven screening of thousands of MOF candidates, have found structures that have good CO_2 selectivity and capacity, even in the presence of water vapor. (Lim et al., 2025)

However, MOFs do not stay stable when they are cycled again and over and exposed to pollutants in the air. (Sanz-Pérez et al., 2016; Shi et al., 2020)

Their large-scale manufacture is expensive and complicated, frequently needing rare metals or difficult synthesis routes.

Another well-known choice is zeolites, which are crystalline aluminosilicates with regular micropores. They are cheap, stable in chemicals, and available. They have high surface areas and well-defined pores. (Choi et al., 2009; Siriwardane et al., 2001) However, moisture significantly reduces their effectiveness, competing directly with CO_2 for adsorption sites. While in some cases a small amount of water can facilitate CO_2 capture by forming weakly bound complexes, in most practical conditions water competes more strongly, blocking pores and reducing the overall CO_2 capacity. This sensitivity to humidity represents a major limitation for the use of zeolites in real-world direct air capture, where air is rarely dry, and maintaining high CO_2 uptake under moist conditions becomes challenging. (Choi et al., 2009).No contemporary sorbent meets all the requirements for an ideal DAC material, which include

excellent selectivity, strong but reversible binding, high working capacity, low regeneration energy, stability over many cycles, and low cost. Shi et al. (2020)(Shi et al., 2020) stress the importance of a systems-level review that looks at more than just sorbent performance measurements. It should also look at lifespan durability, process integration, and the overall economics of the system.

To get over the existing problems and make DAC technologies work on a wide scale in the next few decades, we will need to keep coming up with new ideas in material chemistry, synthesis methodologies, and process design.

1.3 Carbon Nanofibers (CNFs)

1.3.1 Synthesis process

Carbon nanofibers (CNFs) are gaining attention due to their tunable porous structure, area and thermal stability, making them ideal for efficient direct air capture (DAC). Polyacrylonitrile (PAN)-based precursor is one of the most significant carbon fiber precursors. PAN-based carbon fiber makes up about 90% of the world's high-performance carbon fiber market. Their one-dimensional architecture allows for aligned pore systems and efficient gas diffusion, making them ideal for hosting amine groups or other chemisorptive functionalities. (Pohlkemper et al., 2024)

1.3.1.1 Electrospinning

Electrospinning is the most widely used method for producing carbon nanofibers, due to its simplicity, versatility and scalability. The procedure involves injecting a polymer solution, generally polyacrylonitrile (PAN), via a nozzle while applying high voltage to create a fine jet. The solvent evaporates, leading to the formation of solid polymer strands, which are collected into a nonwoven mat of nanofibers. These fibers measure a few tens to a few hundred nanometers in diameter. Electrospinning offers control over polymer solution concentration, voltage, nozzle distance, and humidity, and allows easy addition of materials like graphene or metal oxides, making electrospun carbon nanofibers versatile.

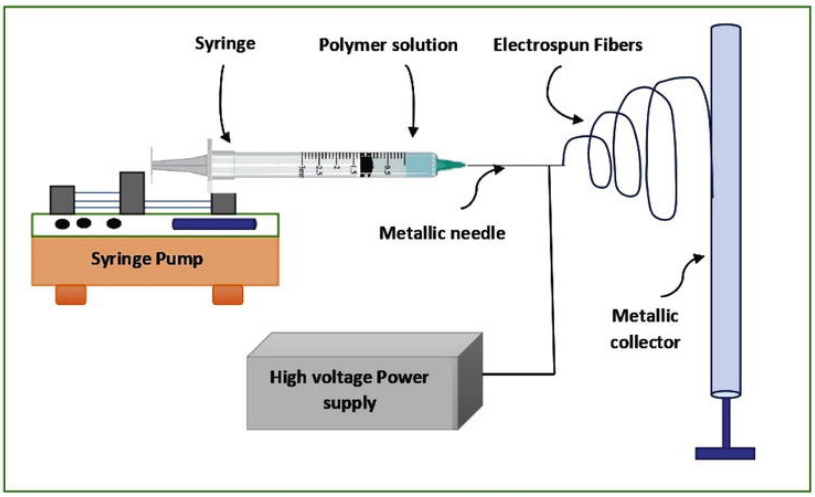

Figure 5: Basic setup of electrospinning (Sharma et al., 2022)

1.3.1.2 Thermal Treatment

After electrospinning, the PAN fibers undergo two key thermal processes: stabilization and carbonization.

Stabilization

The PAN-based fibers are heated in air at 200–300 °C, allowing the polymer chains to undergo oxidative cross-linking and cyclization. This step is critical for preserving the morphological integrity of the fibers during subsequent high-temperature treatment. Poor stabilization may lead to fiber fusion or deterioration of the nanofiber structure during carbonization.

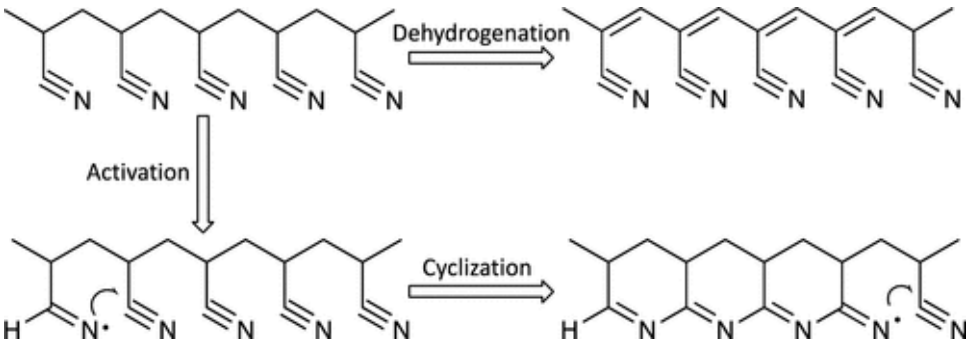

Figure 6: A mechanism of dehydrogenation, activation, and intramolecular cyclization for the stabilization of PAN. (Yao et al., 2024)

Carbonization

The stabilized fibers are further heated in an inert atmosphere, N_2 or Ar for example, at a temperature between 600 and 1100 °C. This process transforms the stabilized structure into a carbon-rich, turbostratic structure while removing non-carbon elements like hydrogen and nitrogen. (Maruccia et al., 2021; Sodiq et al., 2023)

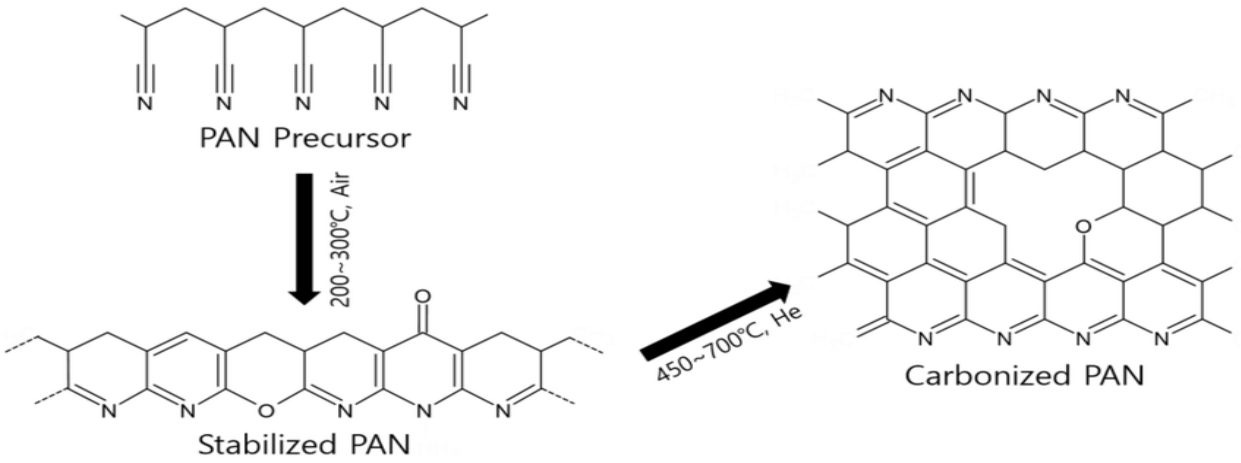

Figure 7: Illustration of the PAN stabilization and carbonization reaction. (Maruccia et al., 2021)

Thermal stabilization and carbonization conditions (temperature, heating rate, duration) have profound effects on the final fiber's surface chemistry, conductivity, and porosity. For example, higher stabilization temperatures encourage the development of pyridinic and quaternary nitrogen groups, which have been linked to improved CO_2 uptake.(Maruccia et al., 2021)

1.3.2 Structure and Surface Properties for DAC Application

The performance of CNFs as solid sorbents in direct air capture is dictated by their structural and surface characteristics.

Surface Area and Porosity

The BET method is the most widely used technique to determine the specific surface area of porous solids. A high specific surface area and optimal pore size distribution, particularly the presence of ultra micropores (0.3-0.7 nm), are essential for maximizing CO_2 adsorption at low pressures as encountered in DAC. Electrospun and activated carbon nanofibers routinely achieve surface areas between 500 and 2000 $m^2\ g^{-1}$, and meticulous adjustment of activation conditions can promote the development of micropores appropriate for CO_2 molecule dimensions (kinetic diameter = 0.33 nm). (Bao et al., 2025)

Studies have shown that the majority of CO_2 uptake in DAC-relevant conditions occurs in these ultramicropores. Too many large mesopores, while facilitating diffusion, often lower selectivity as their size is less complementary to CO_2. (Othman et al., 2024)

Surface Chemistry and Functional Groups

Beyond morphology, the surface functional groups on CNFs or related adsorbents critically influence CO_2 capture. The presence of nitrogen groups can enhance CO_2 adsorption through acid-base interactions and increase binding energies. The content and type of nitrogen groups can be tuned by varying the carbonization temperature and choice of precursor. [21] The oxygen-containing groups also contribute to surface polarity and may enhance physisorption, although their effect is generally secondary to that of nitrogen functionalities.

The performance of the CNFs alone is inadequate for high efficiency DAC, leading to exploration of several surface modification techniques to add functional groups and enhance adsorption capacity.

1.4 Surface Modification Strategies

The surface properties of carbon nanofibers play a crucial role in determining their interactions with CO_2. To enhance their adsorption performance, especially their selectivity and capacity toward CO_2, various surface modification strategies have been employed. These include oxidation, chemical activation and functionalization with specific reactive groups such as amines.

1.4.1 Oxidation

Oxidation is a common pretreatment method used to introduce oxygen-containing functional groups such as hydroxyl (-OH), carbonyl (-C=O), and carboxyl (-COOH) onto the surface of carbon nanofibers.(Kundu et al., 2024) These groups increase hydrophilicity, enhance surface reactivity and provide anchoring sites for further functionalization processes such as silanization. Oxidation can be carried out using strong agents like nitric acid (HNO_3), hydrogen peroxide (H_2SO_4), or sulfuric acid (H_2SO_4). Kundu et al. note that using sulfuric acid in the activation process enhances the porous structure of activated carbon. It is important to note that the porous carbon treated with H_2SO_4 had a CO_2 adsorption capacity of 3.60 mmol g^{-1}, representing a 39.5% enhancement relative to the untreated sample. The material is penetrated

by the acid, resulting in a surface that contains a combination of large and medium-sized cavities.(Kundu et al., 2024)

However, over oxidation can cause excessive weight loss or structural damage, so conditions must be carefully optimized. (Yue et al., 1999)

1.4.2 KOH Activation

KOH activation is a chemical method used to improve the porosity and the specific surface area of carbon compounds. In this process, stabilized CNFs are immersed in potassium hydroxide (KOH) and subjected to elevated temperatures (700-900 ºC). The mass ratio of KOH to carbon significantly impacts the final porosity. Ratios between 1:1 and 4:1 are common, with increased KOH concentration often leading to enhanced surface areas and more microporosity. (Nandi et al., 2023; Williams et al., 2022)

The process involves KOH reacting with the carbon matrix, eliminating disordered areas, and generating new micropores (< 2 nm) and mesopores (2-50 nm). Ultramicropores (0.3-0.7 nm) are also common, making the materials appropriate for CO_2 adsorption at low temperatures. The BET surface area ranges from 500 to 3000 $m^2 g^{-1}$ influenced by variables such as precusor, KOH ratio, and activation conditions. A raised KOH-to-carbon ratio and increased activation temperature often produce more micropores and boost overall pore volume. However, excessive KOH or very high temperatures can cause pore collapse or lead to the formation of larger mesopores, which may decrease CO_2 selectivity.(Nandi et al., 2023; Williams et al., 2022)

Recent investigations by Nandi et al. show that KOH activation significantly enhances adsorptive properties. For example, activating rice husk carbons with KOH increased BET surface area from less than 10 $m^2 g^{-1}$ to 755 $m^2 g^{-1}$, with over 76% micropores, leading to higher CO_2 adsorption (up to 3.13 mmol g^{-1} at 0°C). The isosteric temperatures of adsorption range from 20 to 30 kJ mol^{-1}, indicating strong DAC binding and good regenerability. (Aguilar-Ccuno et al., 2025; Nandi et al., 2023; Wang et al., 2021; Williams et al., 2022)

1.4.3 Aminosilane modification

Functionalizing carbon materials with aminosilane is a targeted chemical strategy designed to enhance adsorption of CO_2 by introducing amine functional groups via covalent attachment of organosilane molecules. The general formula of aminosilane is $H_3Si{-}NH_2$.

The procedure in general involves several steps beginning most often with a surface pretreatment to activate the CNFs. Pretreatment methods such as oxidation introduce reactive hydroxyl, carbonyl, and carboxyl groups that serve as anchor points for silane coupling. Typically, silane coupling agents such as (3-aminopropyl)triethoxysilane (APTMS) are employed due to their bifunctional nature: the alkoxysilane portion, which reacts with the surface -OH, while the terminal amine remains available for CO_2 capture.

1.4.3.1 Chemistry of aminosilane modification

The modification revolves around the condensation reaction between surface hydroxyl groups (from oxidized CNFs) and hydrolyzed alkoxysilane, producing stable Si−O − C. The terminal amine groups (−NH_2 or mixed amine types) remain exposed for CO_2 interaction.(Suresh et al., 2023)

Recent studies show that using silanes with both primary (R−NH_2) and secondary (R_2NH) amine can enhance CO_2 affinity and uptake capacity compared to those with only primary amines.

1.4.3.2 Role of amine groups in CO_2 capture

Amine groups introduced by aminosilane modification act as strong chemisorption sites for CO_2. Under dry conditions, primary or secondary amines bind CO_2 to form carbamates (typically in 2:1 amine-to- CO_2 ratio). Under humid conditions, the presence of water facilitate the formation of carbamates, increasing efficiency to 1:1 ratio and boosting uptake. The amine-CO_2 interaction is highly specific, allowing efficient CO_2 capture even at trace concentrations and offers strong selectivity over N_2 and O_2 common in air.(Suresh et al., 2023)

Recent studies on mesoporous silica grafted with 20-40 wt% APTMS achieved 2.23 mmol g^{-1} at 40 °C with excellent cyclic stability.(Suba et al., 2024) Comprehensive reviews confirm that APTMS-functionalized adsorbents exhibit improved CO_2 capture performance, stability, and regenerability compared to unmodified supports.(Sim & Ruhaimi, 2022)

Although surface modification can substantially enhance CO_2 uptake, the long-term stability of amine-functionalized materials remains a critical concern. Therefore, it is important to examine the degradation mechanisms that limit sorbent lifetime under realistic operating conditions.

1.5 Sorbent Degradation

Long-term CO_2 capture performance depends on the stability of both the amine functional groups and the carbon nanofibers support.

1.5.1 Amine degradation

Amine-functionalized materials are particularly sensitive to degradation. When exposed to high temperatures, oxygen, or contaminants like SO_x and NO_x, amine groups can undergo chemical reaction that either break them down or transform them into less reactive species. This process, often called oxidative degradation, leads to the loss of active amine sites and the formation of byproducts such as amides, nitrosamines and ureas. (Carneiro et al., 2023; S. Zhao et al., 2025)

Recent efforts have shown that substrate-rich Si–OH help reduce oxidative loss via hydrogen bonding, while Al–OH supports are more prone to oxidation but less prone to urea formation.(M. Zhao et al., 2025)

1.5.2 Carbon Nanofibers Degradation

Carbon nanofibers, while generally robust, can also degrade. Repeated exposure to a small amount of oxygen during regeneration steps can slowly oxidize surface carbons, changing pore texture and chemistry. Over time, this degrades CO_2 adsorption performance even though the core fiber remains intact. Thermal gravimetric analyses show changes in weight loss profiles of doped CNFs under inert versus oxidative atmospheres. (Shi et al., 2020)

Although less dramatic than amine degradation, CNFs degradation reduces accessible surface area, impairing subsequent adsorption effectiveness. Recent review stress that long cycle testing under realistic gas mixture is essential to assess this slowly accumulating damage.(Zentou et al., 2025)

1.6 Benchmark Sorbents

Several CO_2 sorbents used in DAC are regarded as benchmarks for their performance and consistency. Notable examples include the commercial resin Lewatit VP OC 1065 and PEI-impregnated carbon nanofibers.

1.6.1 Lewatit VP OC 1065: Structure and DAC performance

Lewatit VP OC 1065 is a commercially available polymeric resin functionalized with primary amine groups, widely recognized as a benchmark material in DAC research. Structurally, it is based on a cross-linked polystyrene backbone functionalized with primary amine groups. These amines are introduced via polymer grafting or immobilisation, enabling strong chemisorption of CO_2 through carbamate formation, a process particularly effective at the ultra-low concentrations of CO_2 found in ambient air. (Low et al., 2023)

According to Sanz-Pérez et al. (2016) (Sanz-Pérez et al., 2016) in circumstances simulating outside air (e.g., 400 ppm CO_2, 25–40°C), Lewatit has exhibited adsorption capabilities between 1.0 and 1.6 mmol CO_2 per gram of resin. Its performance stays consistent across several cycles; however, as is typical with amine-based sorbents, there is a progressive decline in capacity due to oxidative degradation and potential urea production, especially at increased temperatures or in the presence of pollutants.(Fu, n.d.)

1.6.2 PEI-impregnated CNFs: Preparation and Advantages

Polyethylenimine (PEI) impregnated into CNFs is another critical benchmark for DAC, combining the high surface area and tunable porosity of CNFs with the high density of amine groups found in PEI. The preparation of PEI-impregnated CNFs involves combining CNFs with a PEI solution, embedding PEI into the fiber mat, and drying and heating to ensure strong interaction. These PEI-impregnated CNFs have high amine loadings, active CO_2 binding sites, and adsorption capacities even at low temperatures.

This is because PEI's branched structure presents a dense, accessible array of amine groups that chemisorb CO_2 through carbamate or bicarbonate formation.

It is essential to optimize both PEI loading and CNFs pore size because excessive PEI can block the porous network, reducing surface area and accessibility, while too little PEI leaves much of the CNFs potential untapped. Recent studies have shown that tuning the molecular weight of PEI and the characteristics of the CNFs support can lead to substantial improvements in both capacity and stability.(Hack et al., 2022)

This chapter has outlined the principles of adsorption, reviewed current DAC technologies, and highlighted their respective advantages and limitations. Carbon nanofibers (CNFs) emerged as promising sorbents due to their tunable structure, high surface area , and suitability for chemical functionalization. Among various surface modification strategies, aminosilane grafting offers a targeted way to introduce active amine groups and enhance CO_2 capture under ultradilute conditions. However, challenges such as sorbent degradation and stability remain critical barriers to large-scale deployment. These insights provide the basis for the experimental investigations in the following chapters, focusing on the synthesis and functionalization of PAN-based CNFs for DAC applications.

CHAPTER 2:
MATERIALS AND METHODS

CHAPTER 2- MATERIALS AND METHODS

This chapter outlines the experimental approach adopted to design and prepare carbon nanofiber (CNF)-based sorbents for CO_2 capture. It describes the materials used, the synthesis of PAN-derived carbon nanofibers, their subsequent pretreatment and surface modifications, as well as the preparation of benchmark samples for comparison. Finally, it details the characterization techniques employed to evaluate their structural, chemical, and adsorption properties.

2.1 Study area

The research described herein was conducted at Forschungszentrum Jülich (FZ Jülich), a preeminent interdisciplinary research center located in Jülich, Germany. The work was conducted at the Institute of Energy and Climate Research, Electrochemical Process Engineering (IET-1, formerly known as IEK-9), an institution that has gained renown for its contributions to materials science, energy technologies, and climate solutions.

2.2 Materials

The study utilized PAN fibers (from SNC STELLENBOSH NANOFIBER COMPANY) as the primary precursor for carbon nanofiber synthesis,as PAN is the dominant industrial precursor due to its high carbon yield, thermal stability, and ability to form uniform, graphitized nanofibers.(Pohlkemper et al., 2024)

Thermal treatments and processing steps were carried out using laboratory ovens, petri dishes, and ceramic supports. Milling of stabilized fibers was performed with an IKA A10 Basic mill, a METTLER TOLEDO XPR305D5 balance was used for weighting sample masses. The carbon nanofibers were impregnated and pelletized using syringes, pipettes, and spatulas and dimethylformamide (DMF) served as solvent. Polyethyleneimine (PEI) and ethanol were used for the functionalization of the carbon fibers.

Further surface modifications involved potassium permanganate ($KMnO_4$), sulfuric acid (H_2SO_4), hydrochloric acid, and deionized water, with reactions performed in standard larboratory glassware, using a reflux condenser, magnetic stirrer, and heating plate. Filtration was with a vacuum setup and filtration paper.

For silanization, (3-aminopropyl)trimethoxysilane (APTMS) was used. Samples were dried in a Carbolite Gero RETH-E 400/12 oven. CO_2 adsorption measurements were carried out with a

Quantachrome QuadraSorb analyzer (Quantachrome Instruments, USA), using commercial Lewatit VP OC 1065 and PEI-impregnated carbon nanofiber as a reference. Additionally, H_2O adsorption isotherms were measured using a Dynamic Vapor Sorption (DVS) instrument (Surface Measurement Systems, UK)

The Scanning Electron Microscopy (SEM) analysis was performed using an instrument from FEI Company, equipped with a field emission gun (FEG) to achieve high-resolution imaging.

2.3 Methods

2.3.1 Carbon nanofibers Synthesis

2.3.1.1 Precursor Stabilization and Crosslinking

PAN fibers (Figure 8.a) were thermally stabilized in air to make them infusible and prevent melting during subsequent high-temperature processing. The fibers were arranged in glass petri dishes. The stabilization was carried out in an oven under air at 300 °C with a heating rate of 5 °C min^{-1} to encourage controlled cyclisation of nitrile groups. The dwell lasted 4 hours. During this process, the PAN fibers experienced cyclization, dehydrogenation, and oxidation, resulting in the formation of a ladder-like polymeric structure. This structural transformation enhanced thermal stability and prepared the fibers for carbonization. A gradual darkening of the fibers from white to brown was observed. (Figure 8.b)

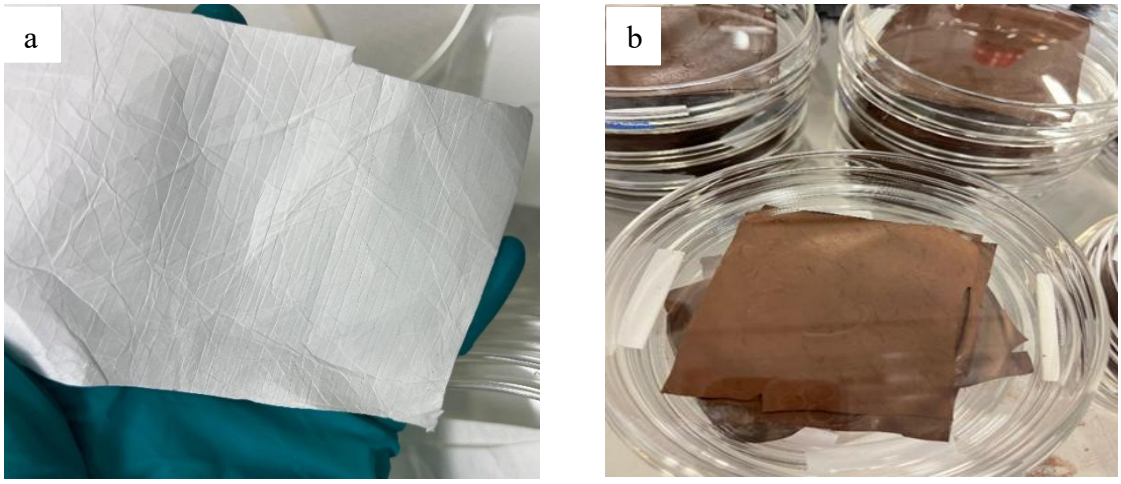

Figure 8: PAN fibers (a) before stabilization, (b) after stabilization

2.3.1.2 Pelletization

To facilitate handling and improve the packing density for subsequent processing, the stabilized fibers were pelletized. These fibers were milled for 2 min 20 s into a fine powder using a laboratory mill (IKA A10 Basic). The powder was then mixed with dimethylformamide (DMF) to form a viscous paste with a PAN content of approximately 10 wt%.

The resulting mixture was extruded using a syringe into fine stands on glass supports. These strands were dried first at moderate temperature (50 °C) for 1 h to evaporate residual solvent, followed by further drying at higher temperatures (100 °C) for another hour to ensure complete removal of DMF. The dried strands were cut into small pellets (Figure 9) of uniform size for carbonization.

Figure 9: Strands of PAN-DMF mixture extruded for pelletization

2.3.1.3 Carbonization process

The stabilized and pelletized PAN samples were carbonized in a tube furnace under a continuous argon flow (approximately 50 Nl h^{-1}) to create an oxygen-free atmosphere and prevent combustion. The temperature was gradually increased to 1100 °C with a heating rate of 300 °C/h and maintained for 3 hours to ensure complete carbonization. After the process, the samples were allowed to cool to room temperature. This treatment transformed the precursor into robust, porous carbon nanofibers with a characteristic black appearance. (Figure 10)

Figure 10: Carbon nanofibers after carbonization.

2.3.2 Pretreatment process

To optimise the properties of the sorbents, two different pretreatment strategies were applied:

- Oxidation of carbonized fibers to introduce oxygen-containing functional groups
- KOH activation of stabilised PAN fibers prior to carbonization, followed by oxidation to enhance porosity and introduce reactive surface groups.

2.3.2.1 Oxidation

The oxidation of carbon nanofibers was performed to add polar oxygen-containing functional groups. For this process, the CNFs were immersed in an oxidative mixture consisting of potassium permanganate ($KMnO_4$) and sulfuric acid (H_2SO_4), with a ratio of about 1:3 by mass for CNFs to $KMnO_4$, along with a 1M sulfuric acid solution.

The concentrated solution of sulfuric acid (95%) was initially diluted with water. Then, the carbon nanofibers were introduced into the reaction flask, followed by the addition of potassium permanganate and finally the H_2SO_4 solution. The mass ratio of CNF to $KMnO_4$ was 1:3, while the CNF to H_2SO_4 ratio corresponded to 1:0.4

The suspension was stirred continuously at around 80 °C for approximately 4 hours to ensure uniform functionalization. After the reaction, the fibers were rinsed with either dilute hydrochloric acid or oxalic acid to dissolve residual manganese compounds and thoroughly washed with deionized water until a neutral pH was reached.

This process enhanced the surface hydrophilicity and reactive oxygen functionalities of the CNFs, making them more appropriate for future silanization.

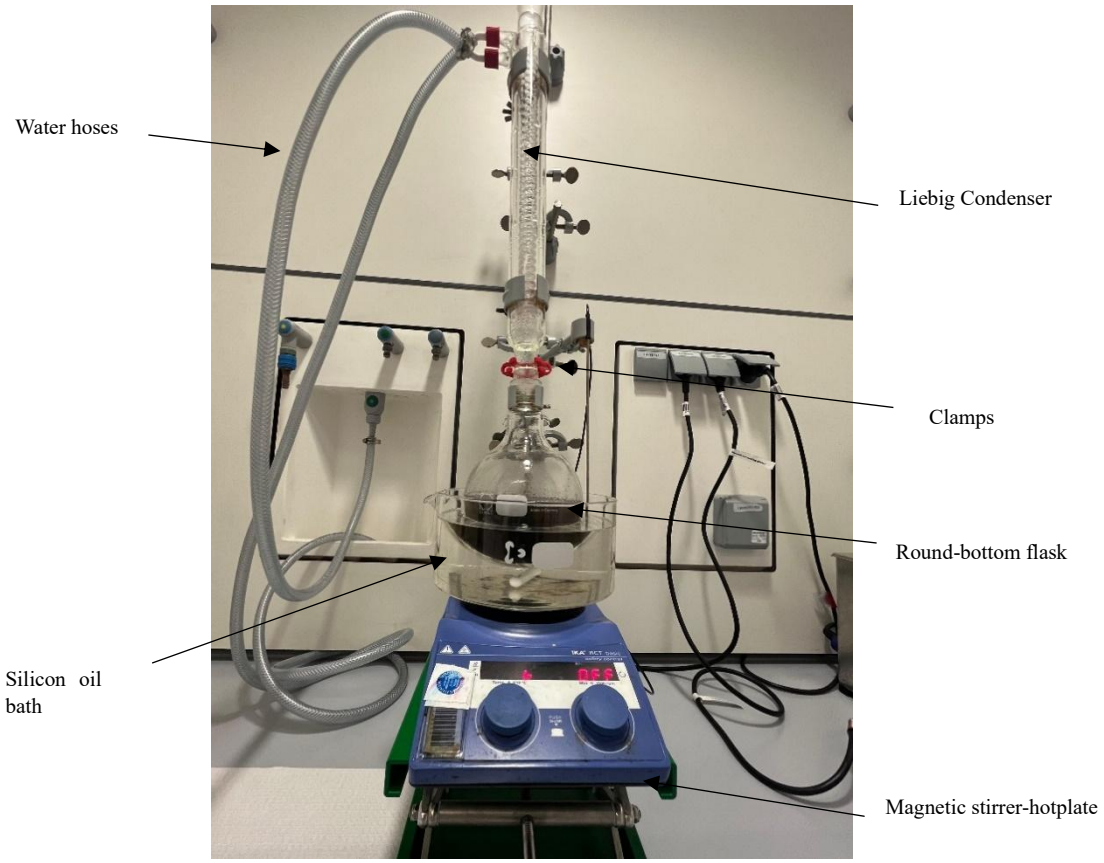

Figure 11: Oxidation setup.

2.3.2.2 KOH activation

KOH activation was performed to enhance the porosity and surface area of the fibers. Stabilized PAN fibers were soaked (Figure 12) in an aqueous potassium hydroxide solution prepared by dissolving solid KOH in water.

The fibers were immersed in this solution for about 2 hours to ensure thorough impregnation. After soaking, they were dried in an oven at 80 °C for 3 hours to reduce moisture. The dried

KOH-impregnated fibers were then carbonized. The sample was heated at a rate of 300 °C until it reached 800 °C, and it was maintained at this temperature for approximately 3 hours under

an Ar flow rate of 50 Nl h^{-1}. This high temperature, widely reported as optimal for KOH treatment, activated the fibers through chemical etching, leading to the formation of a microporous and mesoporous network.(Liu et al., 2024)

After carbonization, the activated fibers were carefully removed from the furnace. White residues were observed on the material surface, which are likely associated with cyanide or potassium-containing byproducts formed during the activation step. To eliminate these residues, the fibers were thoroughly rinsed with deionized water until a neutral pH was achieved, ensuring the effective removal of remaining potassium compounds and other soluble impurities. Finally, the fibers were dried again at 80 °C for a few hours, resulting in KOH-activated carbon nanofibers.

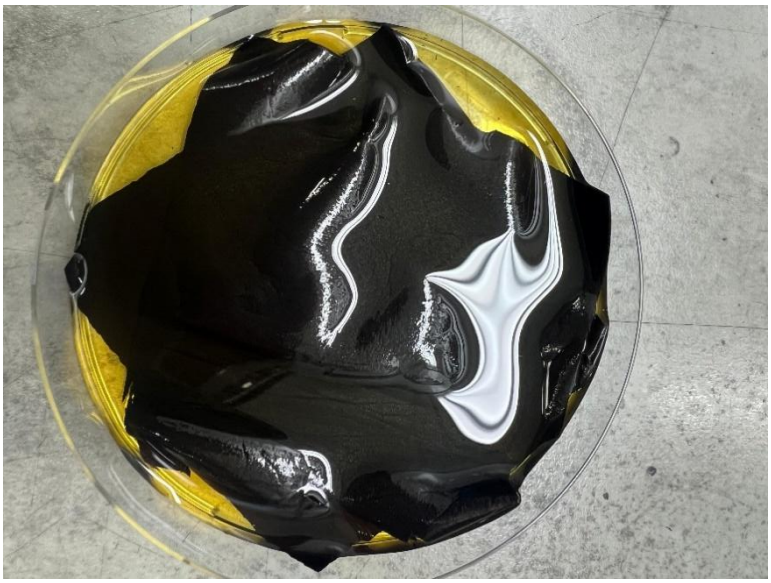

Figure 12: PAN-stabilized fibers soaked in KOH solution

The pretreatment processes prepare the carbon nanofibers by enhancing surface functional groups, thereby improving their reactivity. These modification of the surface chemistry facilitate effective grafting of aminosilane molecules in the subsequent treatment step.

2.3.3 Surface modification with APTMS

To introduce amine functionalities, various pretreated carbon nanofibers samples were functionalized with (3-aminopropyl)trimethoxysilane (APTMS) via silanization process. This modification was applied to oxidized CNFs and KOH-activated and oxidized CNFs.

For most samples, the APTMS was pre-hydrolysed in water for 1 hour at room temperature before contact with the CNFs. One oxidized CNF (sample UOS_1) was treated without this hydrolysis step, allowing direct interaction between unhydrolyzed APTMS and the CNF surface.

Following the hydrolysis step, the CNFs were introduced into the APTMS solution and stirred at room temperature for varying reaction times. (Table 1)

Table 1: Summary of APTMS surface modification conditions for CNF samples

Sample	**Pretreatment Type**	**APTMS Pre-Hydrolysis (1 h in water)**	**Reaction Time with CNFs**	**Reaction Temperature**	**Drying Conditions**
UOS_1	Oxidized CNFs	No	1 h	Room temperature	60 °C, 12–18 h
UOS_2	Oxidized CNFs	Yes	1 h	Room temperature	60 °C, 12–18 h
UOS_3	Oxidized CNFs	Yes	16 h	Room temperature	60 °C, 12–18 h
AOS_1	KOH-activated +oxidized CNFs	Yes	1 h	Room temperature	60 °C, 12–18 h
AOS_2	KOH-activated +oxidized CNFs	Yes	20 h	Room temperature	60 °C, 12–18 h

After silanization, the suspensions were filtered and rinsed thoroughly with deionized water to remove unreacted silane. The samples were then dried at 60 °C for 12–18 h to ensure complete condensation and stabilization of the grafted layers.

This procedure yielded APTMS-functionalized CNFs with varying amine loadings, enabling investigation of the effect of reaction time and pretreatment on CO_2 adsorption performance.

2.3.4 Benchmark Preparation

Impregnation of Carbon Nanofibers with PEI

The impregnation step was carried out to introduce amine functionalities onto the surface of the CNFs, thereby enhancing their affinity for CO_2. For this process, dried CNF powder was placed in a clean beaker, and a polyethyleneimine (PEI)-ethanol solution was prepared at a volume ratio of 1:2 (PEI:Ethanol). The PEI solution was then added to the CNF powder in an amount sufficient to achieve a uniform coating.

To ensure thorough mixing and uniform distribution of the PEI throughout the nanofiber matrix, syringes were used to combine the CNFs and the solution. The mixture was carefully homogenized until a consistent texture was achieved, indicating that the polymer had been evenly impregnated into the porous structure of the carbon nanofibers.

Once the impregnation was complete, the resulting material was pelletized (Figure 13). The pellets were then set aside for further characterization and testing, particularly for their CO_2 adsorption properties. They served as a benchmark sorbent for performance comparison with APTMS-modified CNFs and Lewatit VP OC 1065.

Figure 13: PEI-impregnated CNFs.

A comprehensive set of characterization techniques is utilized to assess the structural, chemical, and adsorption properties of both the prepared CNFs and the benchmark sorbents. These analyses provide critical insights into material performance and enable direct comparison between samples.

2.3.5 Characterization Techniques

2.3.5.1 Scanning Electron Microscopy (SEM) and Energy-Dispersive X-ray Spectroscopy (EDX)

The surface morphology of the sorbents was examined using Scanning Electron Microscopy (SEM) equipped with a field emission gun (FEG) to achieve high-resolution imaging. (FEI Company, USA).For analysis, small amounts of the sample were mounted in aluminum stubs using conductive carbon tape to ensure stability and minimize charging effects. Imaging was performed under an accelerating voltage of 5 kV, with a working distance of 9.9 mm and a spot size 2.0, providing a balance between surface resolution and signal intensity.

Energy-Dispersive X-ray Spectroscopy (EDX), integrated into the SEM system, was employed to determine the elemental composition of the samples. This enabled verification of surface modifications by detecting characteristic signals, such as silicon from APTMS grafting and nitrogen from amine-containing groups. By combining SEM imaging with EDX elemental mapping, it was possible to correlate morphological features with local chemical composition at the microscale. The analysis was conducted for all samples. With the exception of AOS_1, which could not be examined due to an instrumental failure prior to its scheduled measurement.

2.3.5.2 Thermogravimetric Analysis (TGA)

Thermogravimetric analysis was conducted using a STA 449 F1 Jupiter, (Netzsch GmbH, Germany) to examine the thermal stability and composition of the samples. A small amount of sample was placed in an alumina crucible within the TGA instrument. The measurement was carried out under a N_2 atmosphere, with a constant flow rate of 50 mL min^{-1} to avoid oxidation during heating.

The analysis began at 30 ºC, and the temperature was ramped to 120 ºC, where the sample was held for 1 h to ensure complete removal of physically adsorbed water and residual solvents. After the isothermal hold, the temperature was increased to 1000 ºC at a heating rate of 10 K min^{-1}.

2.3.5.3 Static Manometric Analysis

The CO_2 adsorption capacity of the samples was determined using a Quantachrome QuadraSorb analyzer (Quantachrome Instruments, USA) (Figure 14.a) based on static manometric method. This method measures the gas uptake at equilibrium as a function of

pressure, producing isotherms that indicate the materials' affinity and capacity for carbon dioxide.

Prior to measurement, each sample was outgassed at 120 °C for 1.5 hours using 3P Instruments Micro 300 C (Quantachrome Instruments, USA) (Figure 14.b). This pretreatment removed physically adsorbed moisture and contaminants, ensuring that the adsorption date reflected only CO_2 uptake.

Measurements were conducted under controlled temperature and pressure conditions to generate CO_2 adsorption isotherms for unmodified, oxidized, KOH-activated CNFs, APTMS-modified CNFs, PEI-impregnated CNFs, and the commercial benchmark Lewatit VP OC 1065.

The amount of gas adsorbed was calculated from pressure changes using the ideal gas law:

$$n = (Pi - Pf)V \div RT \qquad (1)$$ (*The Ideal Gas Law*, n.d.)

where n is the number of moles adsorbed, Pi and Pf are the initial and final equilibrium pressures, V is the free space volume of the sample cell, R is the universal gas constant, and T is the temperature. The adsorption capacity was then normalized by the sample mass to obtain adsorption capacity in mmol g^{-1}

In addition to CO_2 adsorption, pore size distribution was determined from Ar adsorption isotherms at 87 K using the 3P Micro device. Argon was chosen instead of N_2 because it does not have a significant quadrupole moment, which avoids specific interactions with the surface functional groups and gives more reliable information for microporous materials.(Thommes et al., 2015c) Pore size distribution was calculated from the adsorption branch of the isotherm using the Density Functional Theory (DFT) method integrated in the 3P Micro Software.

The BET surface area model was applied to the isotherm data to calculate the monolayer adsorbed gas volume by the following equation:

$$\frac{1}{v[(p_0/p) - 1]} = \frac{c - 1}{v_m c}\left(\frac{p}{p_0}\right) + \frac{1}{v_m c} \qquad (2)$$ (Lundstedt, 2019)

From the monolayer adsorbed gas volume, the total and specific surface area can be determined:

$$S_t = \frac{v_m N s}{V} \quad (3) \quad \text{(Lundstedt, 2019)}$$

St = total surface area of sample material

v_m= monolayer absorbed gas volume

N = Avogadro's number = 6.02 x 1023 molecules/mol

s = cross-sectional area of adsorbed gas molecule

V = molar volume of adsorbed gas

$$S_{BET} = \frac{S_t}{a} [=] \text{ m}^2/\text{g} \quad (4) \quad \text{(Lundstedt, 2019)}$$

S_{BET} = specific surface area

a = mass of sample

Figure 14: (a) 3P Micro 300 for outgassing, (b) QuadraSorb device for CO_2 adsorption isotherms

2.3.5.4 Dynamic Gravimetric Analysis

Water vapor adsorption behavior was assessed using a Dynamic Vapor Sorption (DVS, Germany) analyzer. Prior to measurement, each sample was carefully weighed and loaded into the DVS sample holder. Before the adsorption step, the samples underwent a thorough

pretreatment under vacuum (< 0.05 Torr) using a turbo pump. The temperature was raised to 120 °C and maintained for 3 hours, with the turbo pump applied during the final 2 hours to ensure complete removal of moisture and volatile contaminants. After degassing, the samples were allowed to cool naturally to room temperature over a period of approximately 2–3 hours.

The sample was then exposed to water vapor at a rate of 20 ml min^{-1}. It was left to equilibrate until the mass variation stabilized at each designated humidity level. Indicating that adsorption equilibrium had been reached.

Throughout the experiment, the DVS system continuously recorded the mass change of the samples. Once the sample masses no longer changed, the water pressure could be further increased. By looking at the vapor uptake for different humidities, an isotherm could be created, with each point corresponding to the H_2O uptake at a given humidity.

At the end of the measurement, the instrument gradually reduced the humidity back to 0 %. This allowed the sample to release any adsorbed moisture, so its desorption behavior could be measured as well.

2.3.5.5 Dynamic Column Breakthrough Analysis

The dynamic adsorption performance of the Lewatit and 33 wt% PEI-CNF, was evaluated using the 3P mixSorb SHP analyzer. A fixed amount of the samples was packed into the adsorption column within the mixSorb system. The gas mixture of CO_2 and N_2 was passed continuously through the column at a certain flow rate. By plotting the outlet CO_2 concentration versus time, the breakthrough curve was generated, showing the point at which the adsorbent becomes saturated and CO_2 starts to appear in the effluent. From this curve, parameters such as adsorption capacity, breakthrough time, and kinetic behavior were determined.

This chapter has detailed the materials, the synthesis routes, and characterization methods employed to develop and study carbon nanofiber-based sorbents for direct air capture. The procedures outlined, including thermal treatment, activation, and surface functionalization, were designed to tailor both the structural and chemical properties of the fibers. The characterization techniques described will provide the necessary insights into morphology. Porosity, and surface chemistry, ensuring a comprehensive evaluation of their adsorption performance. These methods establish the experimental foundation for the results and discussion presented in the following chapter.

CHAPTER 3:

RESULTS AND DISCUSSIONS

CHAPTER 3- RESULTS AND DISCUSSIONS

In this chapter, the structural, morphological, textural, and adsorption properties of the prepared aminosilane-modified carbon nanofibers (CNFs) were evaluated and compared with Lewatit VP OC 1065 and PEI-impregnated CNFs. The aim was to investigate how surface functionalization influences CO_2 adsorption capacity, selectivity, and stability, particularly under conditions relevant to direct air capture (DAC). Comprehensive characterization techniques, including Scanning Electron Microscopy (SEM) coupled with Energy-Dispersive Spectroscopy (EDX), Argon (Ar) physisorption for BET surface area analysis, CO_2 and H_2O adsorption isotherms, Thermogravimetric Analysis (TGA), and dynamic column breakthrough experiments, were employed to establish correlations between morphology, surface chemistry, porosity, and adsorption performance.

3.1 Carbon Nanofiber Oxidation

SEM and EDX were used to examine changes in fiber morphology and elemental composition. Thermogravimetric Analysis (TGA) revealed the stability and nature of surface functionalities introduced by oxidation. Adsorption-desorption measurements (BET analysis) of Ar 87 K were carried out to assess changes in surface area and porosity. Finally, the impact of oxidation on H_2O adsorption performance was assessed to establish the baseline properties of the oxidized materials.

3.1.1 Morphological and Elemental Analysis (SEM, EDX)

SEM analysis (Figure 15) showed pronounced changes in surface morphology after oxidation with H_2SO_4/$KMnO_4$.

After analysis, the unmodified CNFs (U_CNF) showed a relatively smooth surface (Figure 15.a). Upon oxidation with sulfuric acid and $KMnO_4$, the fiber's (O_CNF) surface became rougher (Figure 15.b), likely due to the introduction of oxygen-containing functional groups, which also increase the hydrophilicity of the surface. A partial dissolution of the fibers was observed, indicating that the oxidative treatment induced structural collapse in some regions.

These observations are consistent with the mass loss of approximately 10 wt% recorded after the process.

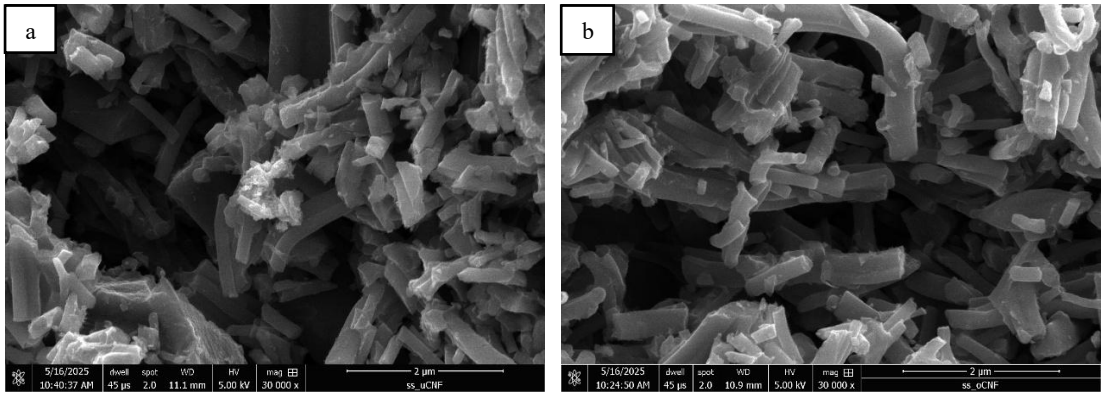

Figure 15: SEM image of CNFs (a) unmodified and (b) oxidized with $KMnO_4$.

EDX analysis (Table 2) confirmed an increase in oxygen content from 0.1% to 1% after the oxidation. No residual manganese Mn was detected, confirming effective removal of Mn-based oxidation byproducts. In contrast, the nitrogen content increased from 0.8 to 1.4 at%. This might be because the oxidative treatment brought out nitrogen functionalities that were already in the fiber structure or because new nitrogen-containing groups formed during the treatment. Another reason might be that the carbon was selectively removed.

Table 2: Elemental composition of CNFs determined by EDX analysis.

Sample	C(at%)	N (at%)	O(at%)
Unmodified CNFs	99.1 ± 4.9	0.8 ± 0.1	0.1 ± 0.03
Oxidized CNFs	97.6 ± 4.8	1.4 ± 0.15	1.0 ± 0.08

The values are reported as mean atomic percentage (at%) ± standard deviation, where the errors reflect the uncertainty associated with EDX quantification

While the morphological and elemental analyses confirm the successful introduction of oxygen functionalities, thermogravimetric analysis provides complementary information on the thermal stability of the oxidized fibers.

3.1.2 Thermogravimetric Analysis (TGA)

The thermal behavior of the unmodified and oxidized CNFs is shown in Figure 16. As expected for a fully carbonized material (carbonization temperature 1100 °C), the unmodified CNFs remained remarkably stable with only a minor weight loss below 150 °C. This slight decrease is most likely associated with the slow decomposition of residual heteroatoms or desorption of physically adsorbed moisture, a phenomenon widely observed in high-purity carbon nanomaterials.

In contrast, oxidized CNFs experienced a notable weight loss (around 9 wt%) with an initial step below 150 °C, attributed to the release of adsorbed H_2O, which indicates the material's hydrophilic nature, as noted by Zygouri et al. (2023). This mass loss is followed by a gradual decrease in mass between 200 and 600 °C. This significant loss is related to the decomposition of oxygen-containing groups like carboxyl, hydroxyl, and carbonyl that were added during the H_2SO_4/$KMnO_4$ treatment. As shown in the J. Phys. Chem. C study (2016) (Liang et al., 2016), carboxyl and hydroxyl moieties typically decompose around 200-400 °C, with more stable groups breaking down later.

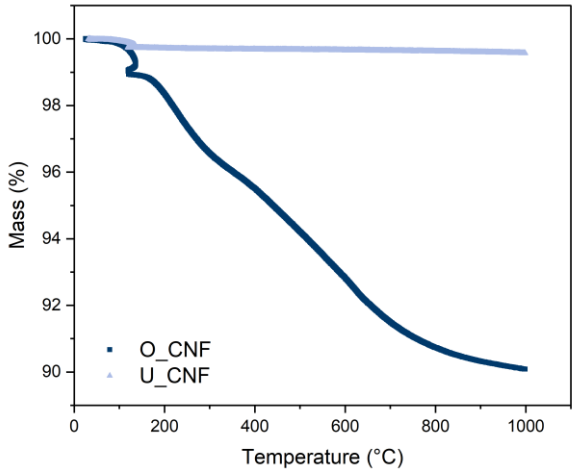

Figure 16: TGA analysis for unmodified and oxidized CNFs.

Thermogravimetric analysis reveals that the introduction of these functionals groups increases the hydrophilicity of the oxidized CNFs while simultaneously reducing their thermal stability. BET surface area and porosity provide a complementary characterization method to analyse the structural effects of this oxidation process.

3.1.3 BET surface area, pore size distribution

After oxidation with H_2SO_4/$KMnO_4$, the BET surface area of CNFs increases from 7.8 $m^2\ g^{-1}$ to 77.6 $m^2\ g^{-1}$ (Figure 18.a). This high increase shows that the oxidation changed the fiber's structure quite a lot, making the surface rougher and inducing pores. The pore size distribution (Figure 18.b) analysis supports this, revealing that O_CNF displays slightly elevated pore volume within 1-2 nm range compared to the U_CNF, which maintains a very low pore volume and minimal structure in the same region.

This trend is not universal. For example, Han et al. (2018) (Han et al., 2018) reported a decrease in surface area after permanganate oxidation of carbon nanomaterials, attributing it to pore blocking by oxygenated groups and partial collapse of the pore wall. Similar decreases have also been observed by Falco et al. 2021 (de Falco et al., 2021) for acid-oxidized carbons. In contrast, our fibers showed a sharp increase in surface area, suggesting that, rather than simply blocking pores, oxidation may have selectively removed more amorphous or disordered carbon regions. By partially etching the fiber surface, new voids and channels were created, as also supported by the shift in the pore size distribution toward larger (mesoporous) diameters.

Overall, oxidation enhances the surface area and pore characteristics. However, they are still moderate and significantly lower than those obtained via more advanced chemical activation processes. The H_2O vapor uptake pattern was also evaluated to determine the hydrophilicity, as these structural changes can affect the interaction with polar molecules.

3.1.4 H_2O adsorption

The H_2O vapor adsorption at 25 °C (Figure 17) shows a contrast between oxidized and unmodified carbon nanofibers. The unmodified fibers adsorbed negligible H_2O across the entire humidity range, remaining below 0.1 mmol g^{-1} even at 90 % RH. In contrast, the oxidized CNF showed a strong increase in water uptake, reaching 4 mmol g^{-1} at 90 % RH. This higher H_2O uptake confirms the previous thermal and surface analyses, demonstrating that oxidized fibers possess oxygen-containing functional groups that significantly enhance their hydrophilicity. Additionally, the increase in porosity provides more available sites and surface area for H_2O adsorption, further contributing to the higher water uptake.

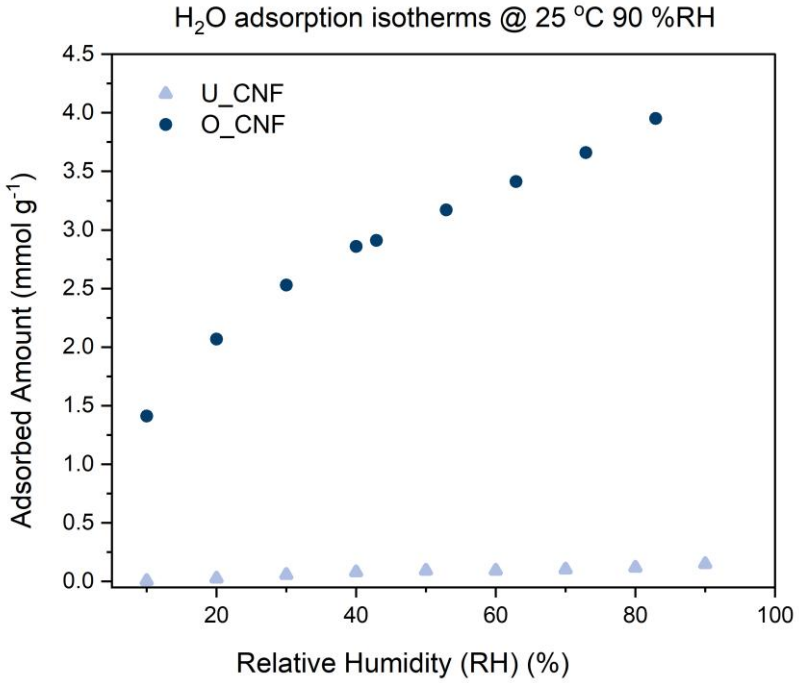

Figure 17: H_2O adsorption isotherms of the unmodified (U_CNF) and oxidized (O_CNF) carbon nanofibers at 25 ºC 90 % RH.

Despite the introduction of oxygen-containing surface groups and a moderate increase in hydrophilicity, oxidation does not greatly improve textural properties such as surface area and porosity. To overcome this limitation, KOH activation step was added to enhance the accessibility of adsorption sites and generate additional porosity.

3.2 KOH activation

To further increase porosity and adsorption capacity, the stabilized CNFs were activated with KOH at 800 °C. This step was expected to change their structure and adsorption properties in a different way than oxidation alone.

3.2.1 BET Surface Area and Pore Size Distribution

KOH activation led to a substantial increase in BET surface area (Figure 18), with values rising from 7.8 $m^2\ g^{-1}$ for the pristine CNFs to 436.91 $m^2\ g^{-1}$ for the samples activated. The pore volume expanded from 0.014 $cm^3\ g^{-1}$ to 0.239 $cm^3\ g^{-1}$, reflecting extensive micropore development. This drastic alteration in pore size distribution (Figure 19) for A_CNF is characterized by a dominant peak at < 2 nm, indicating the creation of abundant microporosity due to the chemical etching effect of KOH on the carbon framework (Gao et al., 2020). Such

behavior is consistent with finding by Fischer et al. (2018) (Fischer et al., 2024)who highlighted how KOH activation controls pore structure and surface chemistry through chemical etching and regeneration cycles.

The AO_CNF exhibited enhanced pore volume across both micropore (around 1 nm) and mesopores (around 3-4 nm) ranges, demonstrating a synergetic effect where KOH activation generates micropores and following oxidation further opens or functionalizes sites

After post-activation oxidation, the surface slightly decreased to 195.87 $m^2 g^{-1}$, which is typical and likely due to partial micropore blockage by oxygen-containing groups introduced during oxidation.

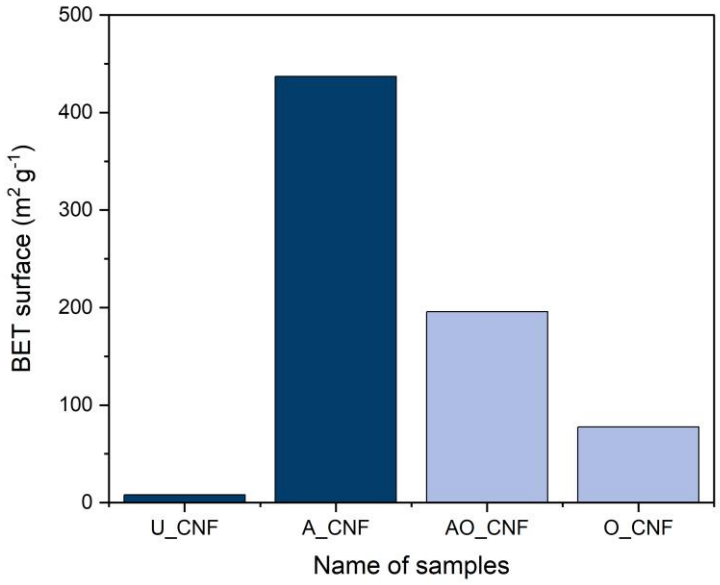

Figure 18: BET surface area of oxidized (O_CNF), activated, and oxidized CNF (AO_CNF), unactivated (CNF) and activated (A_CNF)

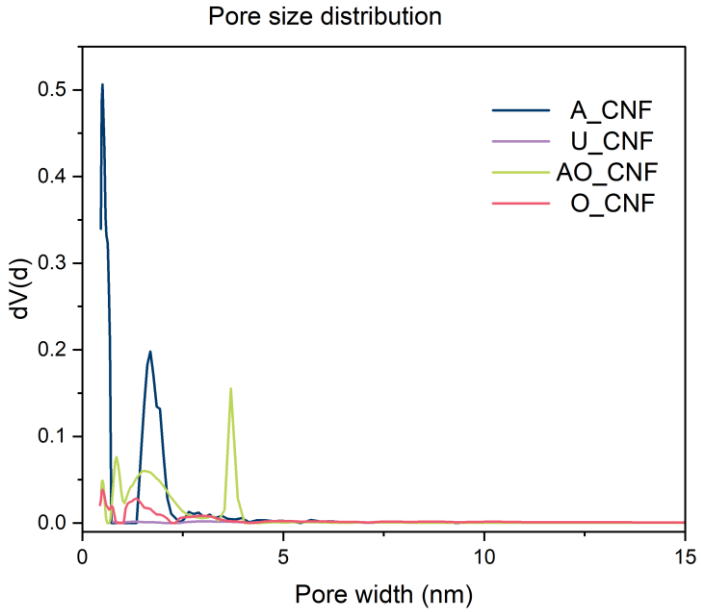

Figure 19: Pore size distribution of A_CNF, U_CNF, AO_CNF, O_CNF

Following the analysis of surface area and pore size distribution, the effect of activation on hydrophilicity and water adsorption capacity was investigated to determine the interplay between porosity and moisture affinity.

3.2.2 H_2O adsorption

The measurement performed at 30 % RH reveals that unactivated CNFs showed negligible H_2O uptake (< 0.1 mmol g^{-1}, Figure 20). Activated CNFs exhibited a moderate increase, reaching 3.8 mmol g^{-1}, likely due to new micropores with hydrophilic edge sites formed during activation. Comparing oxidation effects, the only oxidized sample adsorbed ~2.8 mmol g^{-1} whereas the activated and oxidized sample displayed a much higher uptake of 9.1 mmol g^{-1}.

Isotherms reveal that the activated and oxidized fibers are strongly hydrophilic, with a steep initial uptake at low relative humidity.

The limited uptake of unactivated CNFs is indicative of their low surface area and absence of hydrophilic functional groups. The effect of activation is moderate in the absence of chemical modification, as it introduces micropores that can fit H_2O molecules. Oxidation alone increases H_2O uptake by introducing oxygen-containing groups that serve as primary adsorption sites.

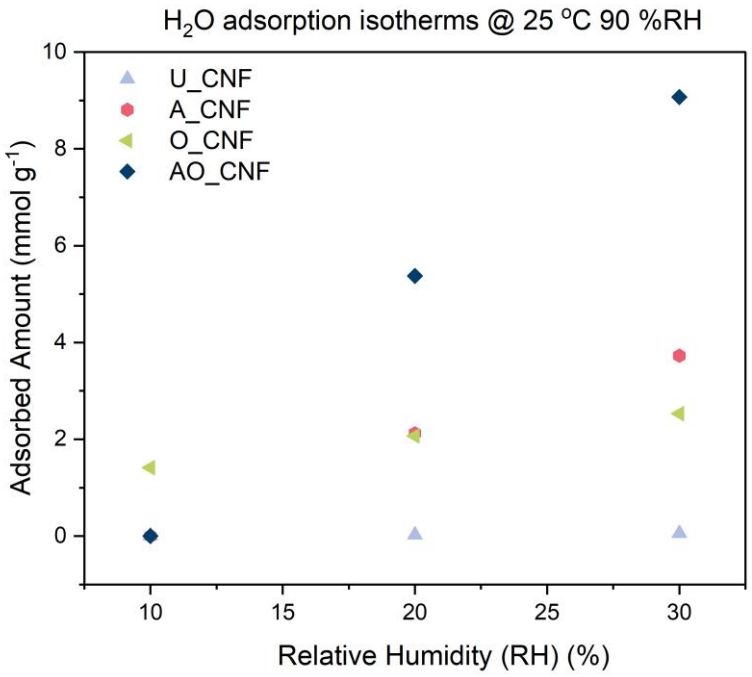

Figure 20: H_2O adsorption isotherms for U_CNF, A_CNF, O_CNF and AO_CNF

All the above data are summarized in Table 3.

Table 3: BET and gas adsorption data for unmodified, activated and activated + oxidized CNFs

Sample	BET ($m^2\ g^{-1}$)	Pore volume ($cm^3\ g^{-1}$)	H2O uptake (mmol g^{-1})
Unmodified	7.8	0.014	<0.1 (90 % RH)
Activated	436.91	0.239	3.8 (30 % RH)
Oxidized	77.6	0.059	4 (90 % RH)
Activated + Oxidized	195.87	0.13	9.1 (30 % RH)

Although U_CNF and O_CNF showed a negligible porosity, the combination of oxidation and KOH activation provided both reactive surface sites and enhanced textural properties. These modifications created an appropriate foundation for the subsequent silanization with APTMS, which was designed to introduce chemisorptive functionalities that are capable of capturing CO_2 at very low CO_2 concentrations (400 ppm) and in the presence of humidity.

3.3 CNFs silanization

To enhance the CO_2 capture capacity of the carbon nanofibers (CNFs), surface functionalization with 3-aminopropyltrimethoxysilane (APTMS) was performed under different conditions.

3.3.1 Effect of Different Silanization Processes

To investigate the influence of functionalization conditions on the structural and adsorption properties of CNFs, five silanized samples were prepared by varying the pre-treatment of the fibers, the hydrolysis of APTMS and the duration of the silanization step (Table 4)

Table 4: Summary of silanization conditions.

Sample	Pre-treatment	APTMS hydrolysis	Silanization time
UOS_1	Oxidation	No	1 h
UOS_2	Oxidation	1 h	1 h
UOS_3	Oxidation	1 h	16 h
AOS_1	KOH activation + Oxidation	1 h	1 h
AOS_2	KOH activation + Oxidation	1 h	20 h

UOS_1: Unactivated, Oxidized and Silanized sample 1

UOS_2: Unactivated, Oxidized and Silanized sample 2

UOS_3: Unactivated, Oxidized and Silanized sample 3

AOS_1: Activated, Oxidized and Silanized sample 1

AOS_2: Activated, Oxidized and Silanized sample 2

To verify the efficiency of the different silanization routes, morphological and elemental analyses were performed to confirm the presence of silicon and nitrogen functionalities.

3.3.2 Morphological and Elemental Analysis (SEM, EDX)

SEM imaging shows a more uniform and lightly roughened surface after silanization, especially for activated and oxidized CNFs, indicating an effective coating (Figure 21).

EDX confirmed successful grafting of APTMS. While pristine CNFs displayed no detectable Si or N, silanized samples showed a clear peak for these elements, with their atomic content increasing with silanization duration. While trace amounts of Mn are commonly observed after strong chemical treatments, their levels should be monitored. The SEM image (Figure 22) of sample AOS_2, showing areas with and without MnO patches, suggests that these MnO patches may block active sites and reduce surface area.

Table 5: Elemental composition of the different silanized samples determined by EDX analysis.

Sample	C (at%)	O (at%)	Si (at%)	N (at%)	Mn (at%)
UOS_1	96.7 ± 4.9	1.7 ± 0.1	0.2 ± 0.0	1.3 ± 0.1	0.1 ± 0.0
UOS_2	85.7 ± 4.9	8.4 ± 0.7	2.0 ± 0.1	3.9 ± 0.4	0.0
UOS_3	93.2 ± 5.0	3.5 ± 0.3	0.9 ± 0.1	2.5 ± 0.3	0.0
AOS_2	79.3 ± 4.8	12.4 ± 0.9	3.3 ± 0.2	5.0 ± 0.5	0.0

The values are reported as mean atomic percentage (at%) ± standard deviation, where the errors reflect the uncertainty associated with EDX quantification.

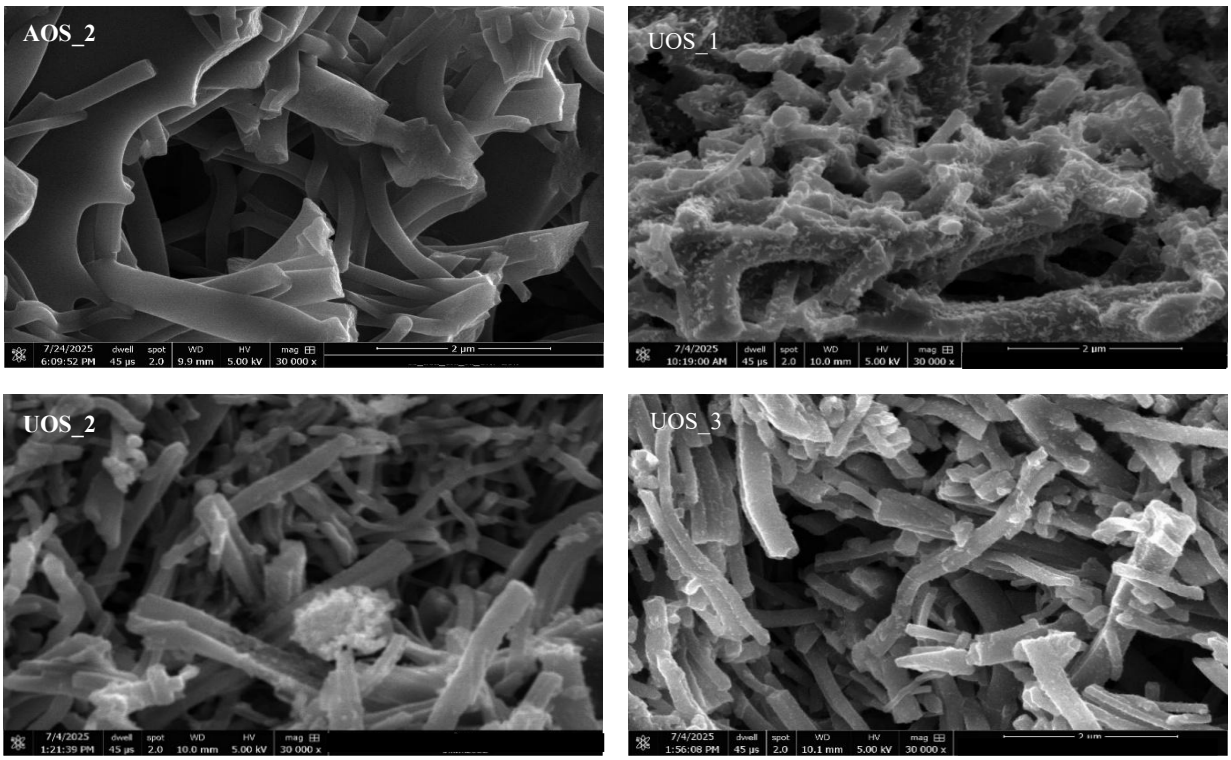

Figure 21: SEM images of all silanized samples except sample AOS_1, due to instrumental failure before the analysis

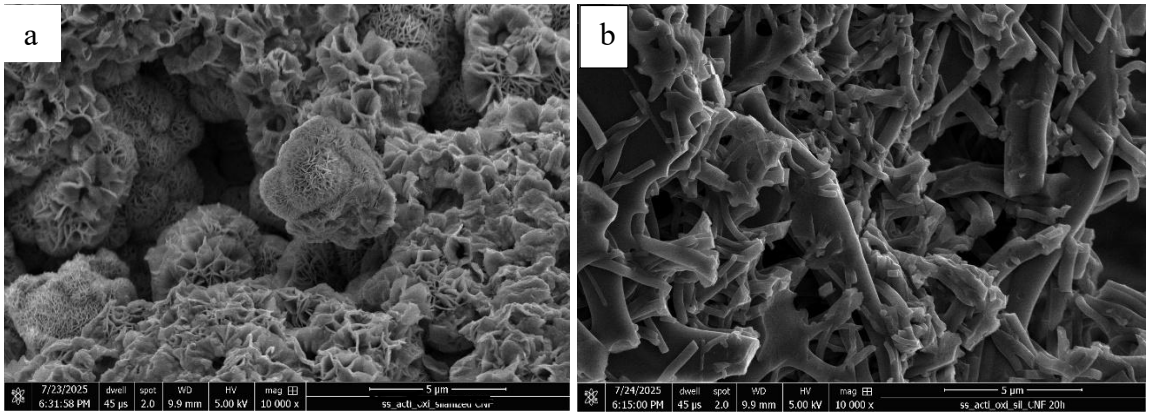

Figure 22: SEM images of sample AOS_2 displaying regions with (a) and without (b) MnO patches.

The MnO patches appear as distinct textured areas on the surface.

After confirming successful functionalization, the influence of grafted amine groups on CO_2 capture capacity was evaluated under relevant conditions

3.3.3 CO_2 Adsorption

CO_2 adsorption isotherms at 25 °C (Figure 23) revealed distinct differences among the samples. The samples UOS_1 to UOS_3 exhibited very low uptakes (less than 0.5 mmol g^{-1}), with isotherms dominated by weak physisorption. In contrast, samples that have been extensively silanized and pre-treated such as AOS_1, particularly AOS_2 exhibited significantly higher capacities (> 0.5 mmol g^{-1}), especially at low pressures (0.1 bar). The type I isotherm shape of sample AOS_2 supports the chemisorption on primary amine groups, as proved by the steep initial uptake. This reflects localized adsorption sites in microporous structure.

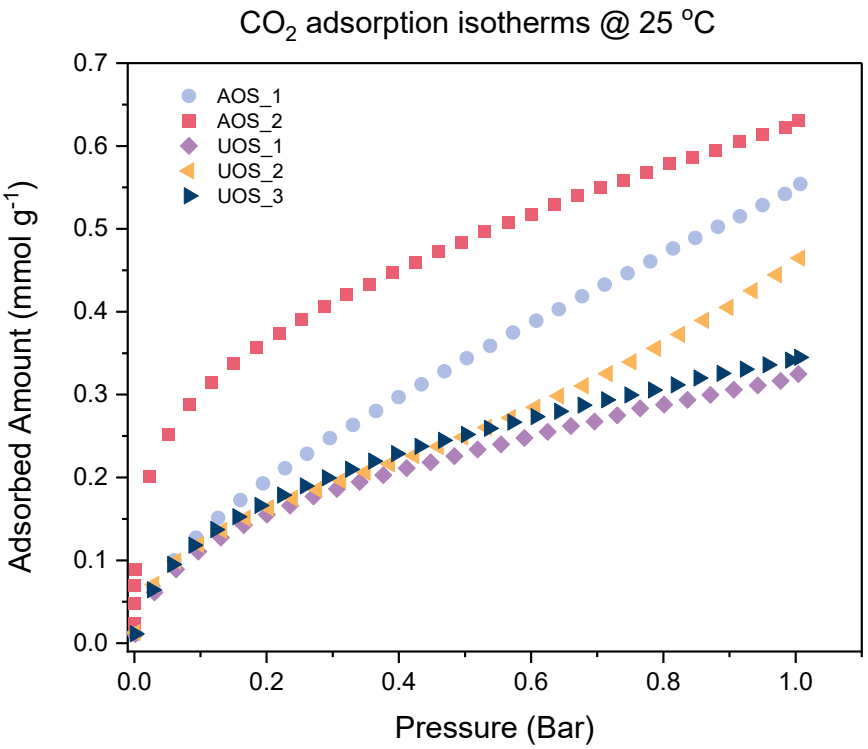

Figure 23: CO_2 adsorption isotherms of all the silanized samples at 25 °C, 400 ppm.

Although sample AOS_2 exhibited the highest CO_2 uptake among all the silanized CNFs (0.65 mmol g^{-1}), it did not exceed 1 mmol g^{-1}. This limitation likely arises from a combination of structural constraints, the presence of residual elements from the activation and oxidation steps, and incomplete grafting. Even though EDX did not quantify Mn, K or Na, these elements are typically introduced during KOH activation and oxidation. Their presence, even at undetectable levels, can occupy anchoring sites for silane grafting, reducing the density of accessible amines. They can modify the local surface charge (for instance, K^+, Na^+), potentially decreasing the nucleophilicity of grafted amines and their reactivity toward CO_2 (Petrovic et al., 2021).

The BET surface area of 58.92 m^2 g^{-1} indicates a strong reduction from the oxidized CNFs (>200 m^2 g^{-1}). This reduction is a clear sign of dense silane grafting, which, while providing amine sites, also blocks micro and mesopores, restricting CO_2 diffusion and reducing the number of accessible adsorption sites. (Samanta et al., 2012)

Trace Mn and S species may create Lewis acid or acidic surface sites. These can interact with CO_2 to form weak carbonate or bisulfide complexes, but such interactions are less reversible than amine-based carbamate formation, limiting the working adsorption capacity. (Chiang et al., 2021)

3.3.4 H_2O adsorption

The unactivated but oxidized and silanized samples (UOS_1, UOS_2) showed a very low H_2O uptake across all relative humidities examined (Figure 24). This limited water adsorption is expected for CNFs with a low surface area and relatively sparse distribution of hydrophilic functional groups, even after silanization. In contrast, the AOS_1 and AOS_2 samples, which underwent both activation and oxidation before silanization, demonstrated a marked increase in water adsorption capacity. The increase in uptake correlates with the vastly increased surface area and microporosity introduced during KOH activation. The silanization and the combination of remaining oxygen functional groups and accessible amines create additional polar sites for H_2O sorption. (Guo et al., 2022)

Interestingly, while their total water uptake is relatively higher than that of the unactivated samples, the shape of the isotherms suggests a difference in the surface character. Amine-functionalized silanes are known to relatively moderate water adsorption compared to a surface dominated by carboxyls and hydroxyls, often yielding a profile that rises steadily with relative humidity but does not reach the levels seen in hydrophilic, non-silanized carbons. (Gebald, 2014)

Similarly, broader reviews of amine-based sorbents emphasize that functionalization strategies increasing surface polarity consistently raise water uptake, even under conditions where CO_2 adsorption is not the focus.

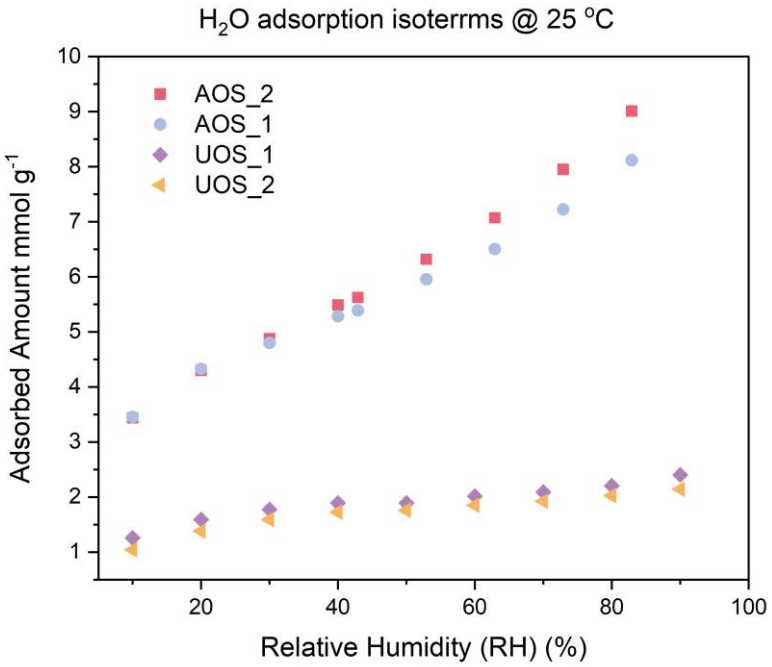

Figure 24: H_2O adsorption isotherms of all the silanized samples at 25 °C

3.4 Comparison with benchmarks

This section compares the performance of the functionalized CNF samples, particularly the AOS_2 sample, with the widely recognized benchmark sorbent, Lewatit VP OC 1065 and the prepared benchmark CNFs impregnated with 33 wt% PEI.

3.4.1 Morphological and Elemental Analysis (SEM, EDX)

The SEM images of the AOS_2 sample (figure 25.a) reveal a highly porous network, consistent with successful surface activation. The rough surface texture suggests efficient APTMS grafting, potentially increasing available adsorption sites while maintaining open gas pathways, an essential feature for fast mass transfer in gas sorption applications. In contrast, the SEM image of Lewatit VP OC 1065 (Figure 25.c) shows a dense resin bead surface. This morphology is typical for polymeric ion-exchange resins, where CO_2 capture occurs primarily through the internal pore network and the accessibility of amine functional groups within the polymer matrix.(Heydari-Gorji et al., 2011)

The 33 wt% PEI-impregnated CNFs (Figure 25.b) exhibit a partially blocked fibrous architecture, where the individual nanofibers remain visible but appear coated with dense PEI layers. This results in a more irregular and possibly obstructed pore structure. Such a non-

uniform coating can limit effective surface area and reduce accessibility of amine sites, especially at higher PEI loadings.

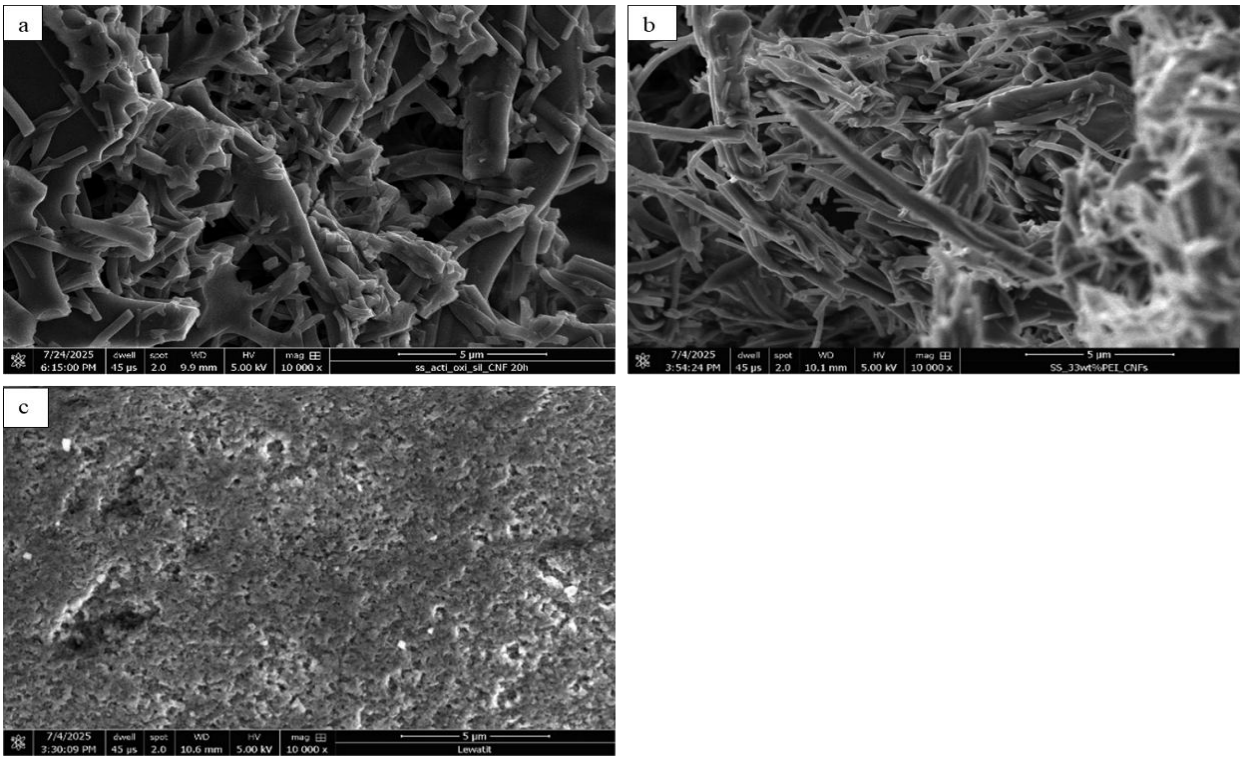

Figure 25: SEM images of (a) AOS_2, (b) 33 wt% PEI-impregnated CNFs, (c) Lewatit VP OC 1065

Beyond surface morphology and composition, textural properties such as specific surface area and pore size distribution provide further insight into differences between the developed CNFs and benchmark sorbents.

3.4.2 BET surface area, pore size distribution

The pore size distribution curves (Figure 26) for AOS_2, Lewatit and 33 wt% PEI-CNFs reveal notable differences in textural features that reflect their distinct material structures.

AOS_2 exhibits a pronounced peak centered around 3-4 nm, indicative of well-developed mesoporosity. This mesoporosity structure likely results from the combined effects of activation, oxidation, and silanization, creating a hierarchical pore network beneficial for rapid mass transfer during the adsorption process. (Sekizkardes et al., 2022) Correspondingly, with a BET surface area of 58.92 m^2 g^{-1}, the AOS_2 sample shows a significantly higher surface area than both benchmarks, Lewatit (38.27 m^2 g^{-1}) and 33 wt% PEI-impregnated CNFs (2.48

m^2 g^{-1}). This suggests that its porous nanofibers structure remains more accessible despite functionalization.

In contrast, Lewatit displays a broader pore size distribution extending into mesoporous (up to ~18 nm), consistent with its polymeric bead structure, designed for facile diffusion of gases and liquids. Although Lewatit's BET surface area is modest, its CO_2 adsorption capacity (see Section 3.4.3) derives largely from the bulk polymer content. The 33 wt% PEI-CNFs sample exhibits a comparatively limited pore volume with a broad, shallow peak, centered below 3 nm, reflecting the nanofiber's microporous backbone partially obstructed by the dense PEI coating. This restricted microporosity corresponds to a much lower surface area, consistent with the BET area of 2.48 m^2 g^{-1}, and highlights the common trade-off in PEI functionalization between pore accessibility and higher amine loading.

The results emphasize the significance of a balance between porosity and chemical functionalization in optimizing sorbent performance, ensuring efficient gas capture through accessible pore architecture

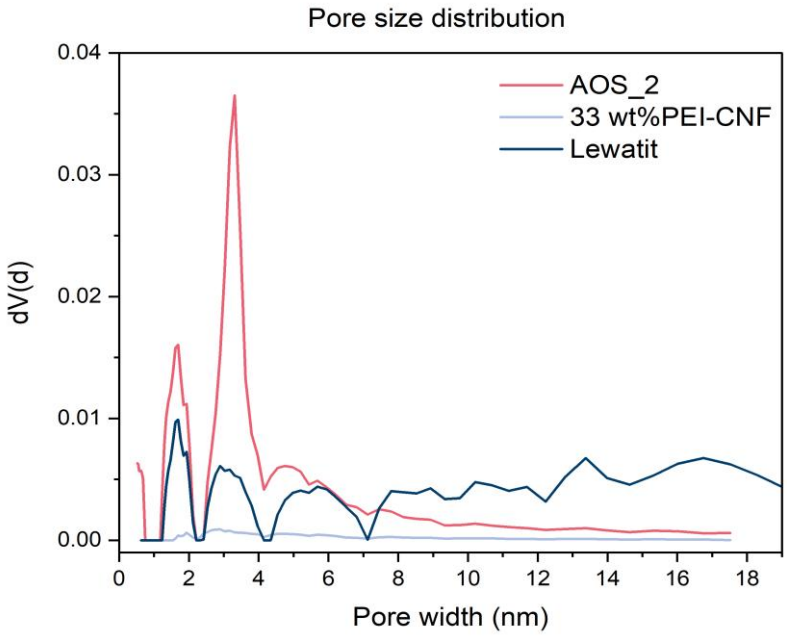

Figure 26: Pore size distribution of AOS_2, Lewatit, 33 wt% PEI-CNFs

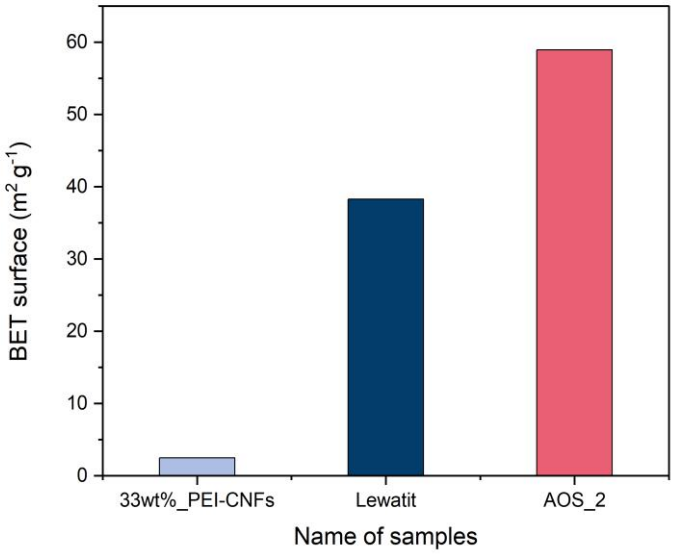

Figure 27: BET surface area of AOS_2, Lewatit and 33 wt% PEI-CNFs

These structural differences directly impact CO_2 uptake, which was therefore examined in detail under dry and humid conditions**.**

3.4.3 CO_2 adsorption

At 400 ppm (DAC conditions), Lewatit (Figure 28) displays the highest CO_2 capacities, reaching loadings 1.7 mmol g^{-1} at 313 K, ~ 2.1 mmol g^{-1} at 298 K and ~3.0 mmol g^{-1} at 273 K. This is consistent with literature reporting its high primary amine density and strong chemisorptive affinity for CO_2 (Young et al., 2021). At low temperatures, adsorption capacity increases due to thermodynamic favorability.

In contrast, the 33 wt% PEI-impregnated CNFs (figure 29) achieved ~0.45 mmol g^{-1} (313K), ~0.75 mmol g^{-1} (298 K) and 0.25 mmol g^{-1} (273 K), values typical for moderate PEI loadings where partial pore blockage and polymer mobility limitations reduce accessible amine sites. (Samanta et al., 2012)

The AOS_2 sample (Figure 30) showed intermediate performance with ~0.60 mmol g^{-1} at 298 K, ~1.15 mmol g^{-1} at 273 K, and ~0.76 mmol g^{-1} at 313 K, outperforming the PEI benchmark at 273K and 313 K but remaining below Lewatit. The reduced capacity may be due to lower amine loading. Additionally, trace MnO_2 residues potentially undetected by elemental analysis could alter surface chemistry by blocking active amine sites or modifying local acid-base interactions.

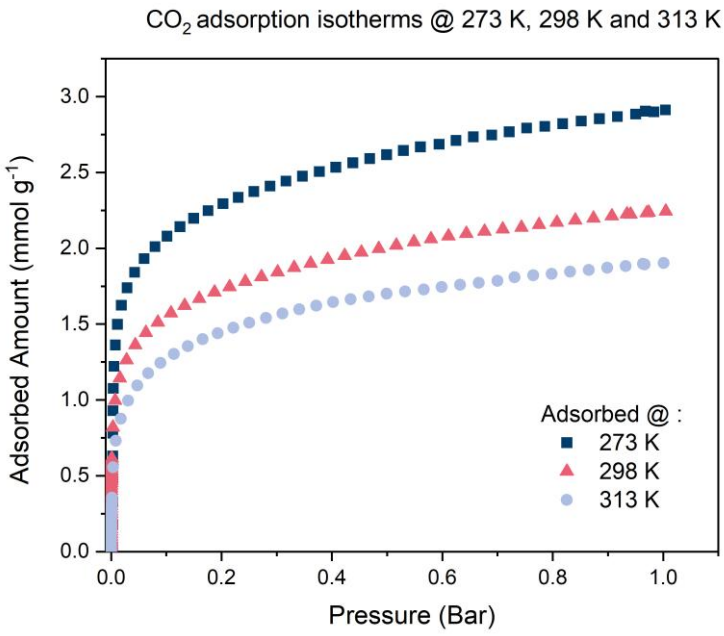

Figure 28: CO_2 adsorption isotherms for Lewatit VP OC at 273 K, 298 K, 313 K

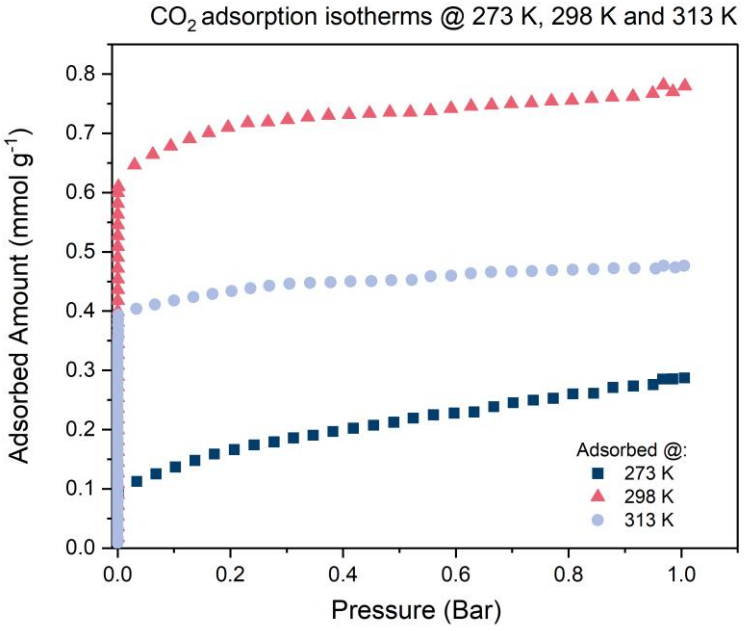

Figure 29: CO_2 adsorption isotherms for 33 wt% PEI-impregnated CNFs

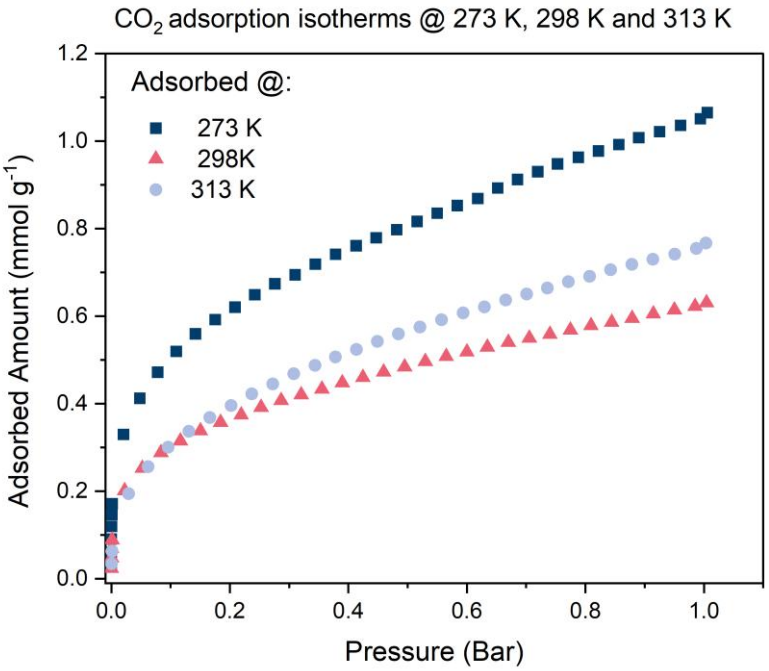

Figure 30: CO_2 adsorption isotherms for AOS_2 at 273 K, 298 K, 313 K

3.4.4 H_2O adsorption

At 298 K and 90 % RH, Lewatit VP OC 1065 adsorbed ~5.75 mmol g^{-1} of H_2O, reflecting its moderate hydrophilicity due to primary and secondary amine groups. Literature on its co-adsorption behavior shows water can enhance uptake via bicarbonate formation, underscoring its affinity for moisture.

The 33 wt% PEI-impregnated CNFs exhibited a much higher uptake of 22 mmol g^{-1}, consistent with literature reports attributing such values to extensive hydrogen bonding networks with water facilitated by the high polymer content. (Veneman et al., 2015) The AOS_2 sample adsorbed ~9.5 mmol g^{-1}, exceeding Lewatit but remaining below the PEI-based sorbent. This intermediate performance can be attributed to the APTMS-derived amine functionalities combined with the relatively open structure, enabling significant water uptake while avoiding the excessive hydrophilicity seen in high-PEI systems.

Trace hydrophilic residues like MnO_2 might also contribute to enhanced polar affinity, thereby supporting its elevated water uptake relative to Lewatit. (Veneman et al., 2015)

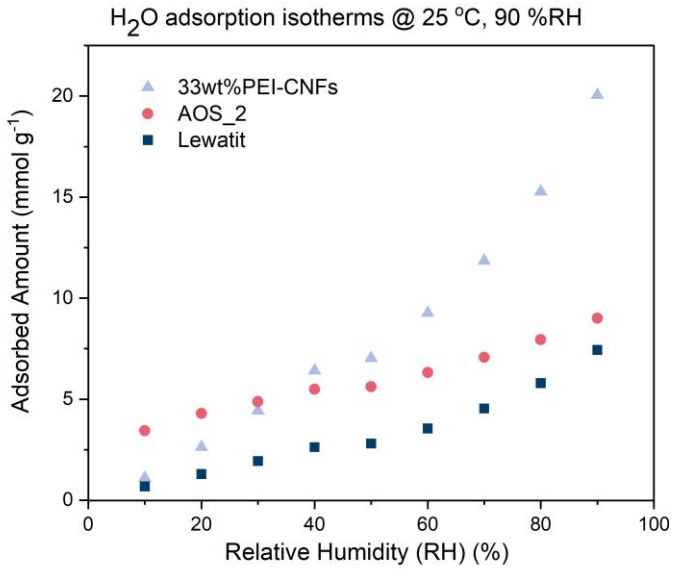

Figure 31: H_2O adsorption isotherms for the AOS_2 sample, Lewatit, and 33 wt% PEI-CNF

3.4.5 Dynamic column breakthrough

The H_2O vapor breakthrough curves reveal differences between Lewatit and 33 wt% PEI-CNFs under different humidity and temperature conditions (Figure 32, Figure 33 respectively) Lewatit exhibits steep breakthrough curves at both 25 °C and 40 °C, with saturation reached within approximately 200 min g^{-1} at 30 % RH and fewer than 300 min g^{-1} even at 70 % RH. These sharp, narrow breakthroughs indicate rapid adsorption kinetics typical of amine resin sorbents with easily active sites. The slight rightward shift of the breakthrough at higher humidity reflects increased water uptake capacity, but overall, the process remains fast and efficient. In contrast, the PEI-CNFs present notably less steep curves, demonstrating slower adsorption kinetics. At 25 °C and 70 % RH, breakthrough extends beyond 1000 min g^{-1} with a gradual increase in outlet concentration, signifying kinetically limited uptake and diffusion, within the more complex fiber matrix. This kinetic limitation is balanced by higher total water uptake as reflected by the delayed breakthrough compared to Lewatit. At elevated temperature with reduced water retention due to thermal effects and accelerated desorption.

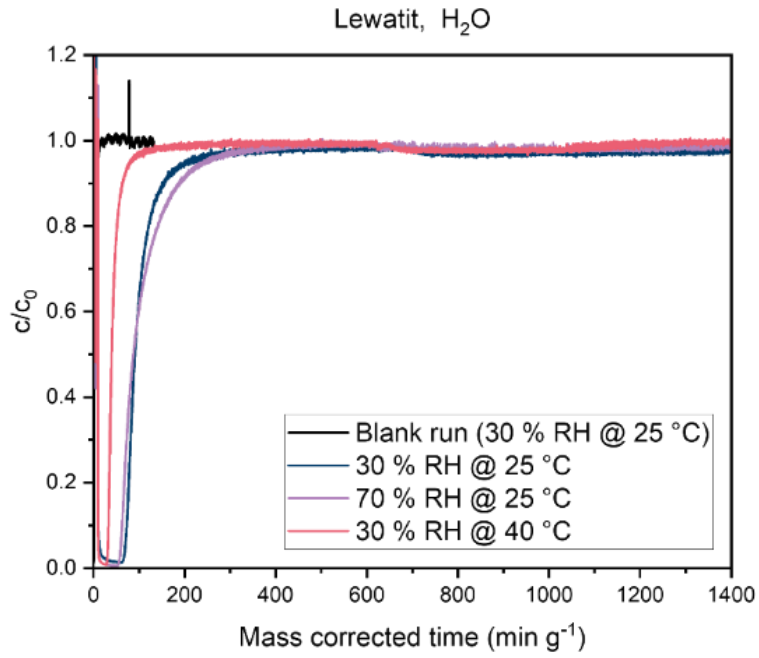

Figure 32: Lewatit H_2O breakthrough curves at 25 ^oC and 40 ^OC

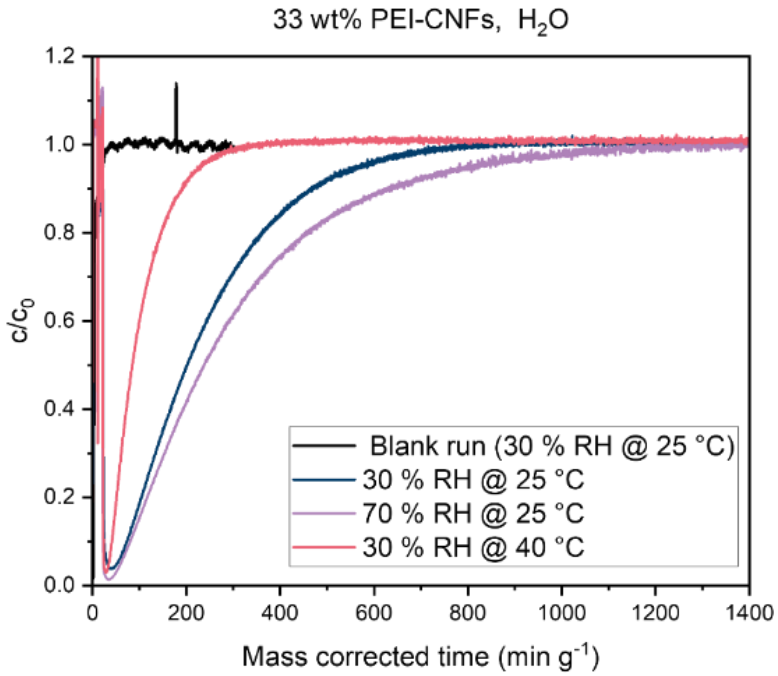

Figure 33: 33 wt% PEI-CNFs H_2O breakthrough curves at 25 °C and 40 °C

Moving to CO_2 adsorption at 400 ppm under pre-humidified conditions, Lewatit at 25 °C shows a clear effect of humidity, wherein higher RH delays the breakthrough. For example, a breakthrough occurs around 600 min g^{-1} at 0 % RH and extends to nearly 1000 min g^{-1} at 70 %

RH. However, raising the temperature to 40 °C results in earlier breakthrough times (approximately 200–400 min g^{-1}) and a less marked influence of humidity on CO_2 retention. Lewatit's breakthrough curves show a steep shape, showing rapid saturation once the sorbent becomes filled.

On the other hand, the 33 wt% PEI-CNFs show considerably longer breakthrough times for CO_2 at both 25 °C (Figure 34) and 40 °C (Figure 35) compared to Lewatit (Figure 36, and Figure 37), indicating a superior adsorption capacity. Similar to Lewatit, increasing relative humidity enhances CO_2 uptake, with the highest RH yielding the longest breakthrough times. The PEI-CNFs showed more gradual breakthrough curves, suggesting differences in adsorption kinetics or sorbent heterogeneity. Even at 40 °C, PEI-CNFs retain a better CO_2 capturing capacity than Lewatit, although breakthrough occurs sooner than at 25 °C.

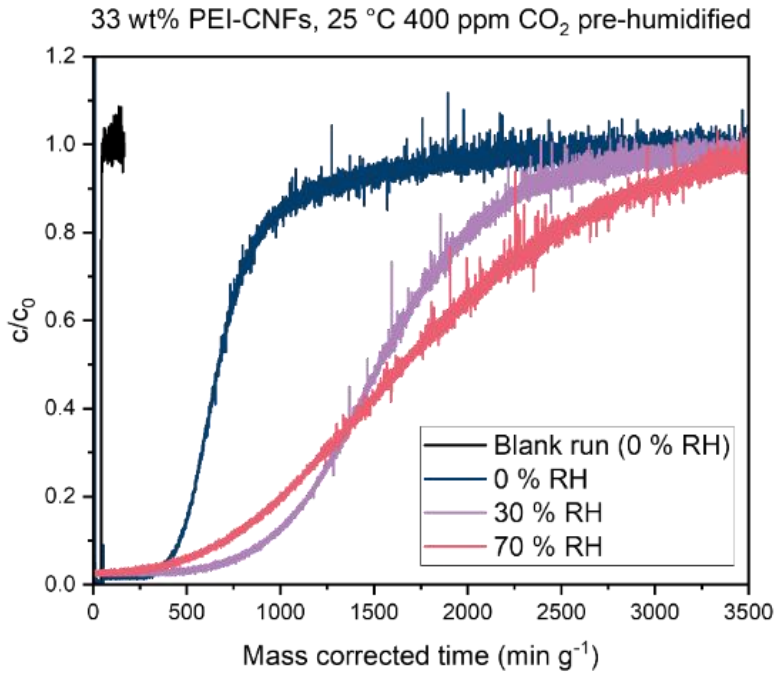

Figure 34: 33 wt% PEI-CNFs CO_2 breakthrough curves at 25 °C

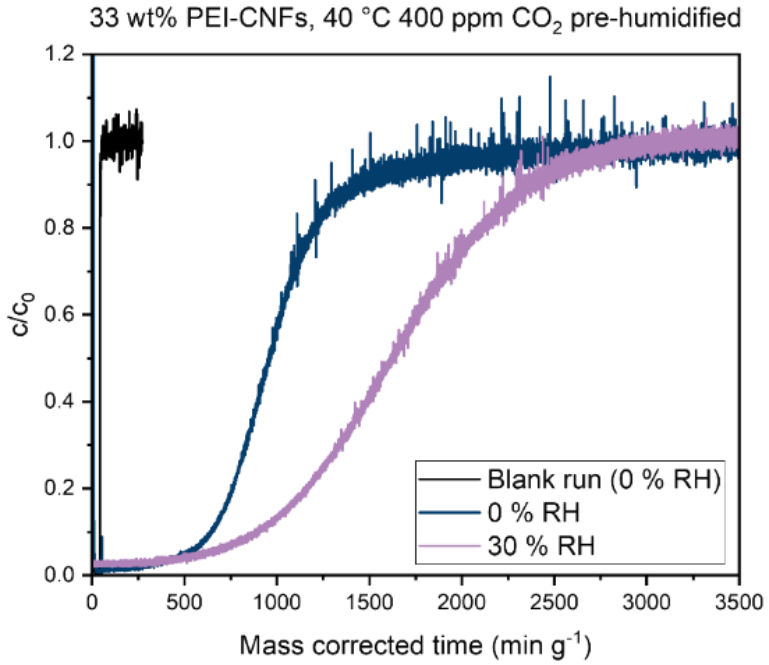

Figure 35: 33 wt% PEI-CNFs CO_2 breakthrough curves (BTC) at 40 ºC.

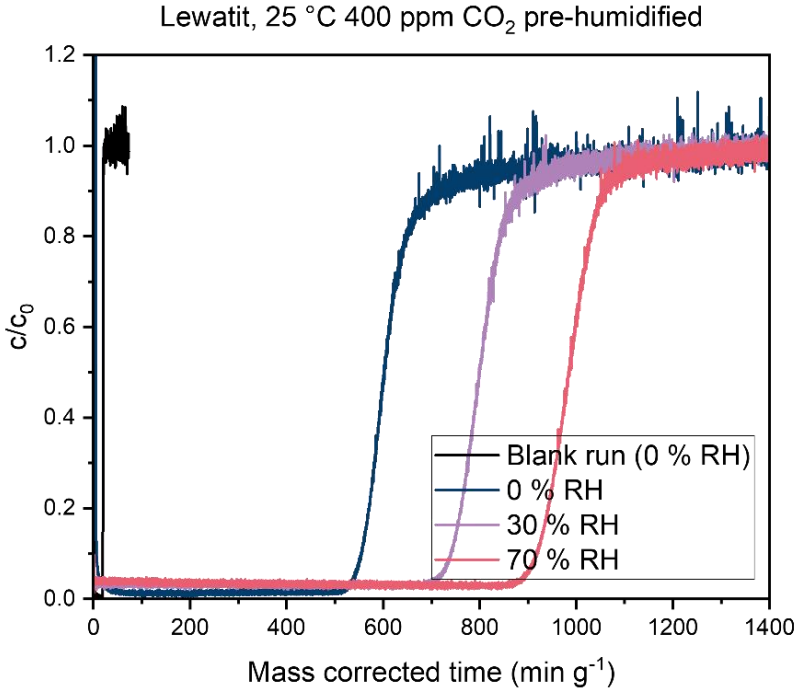

Figure 36: Lewatit VP OC 1065 CO_2 breakthrough curves (BTC) at 25 ºC

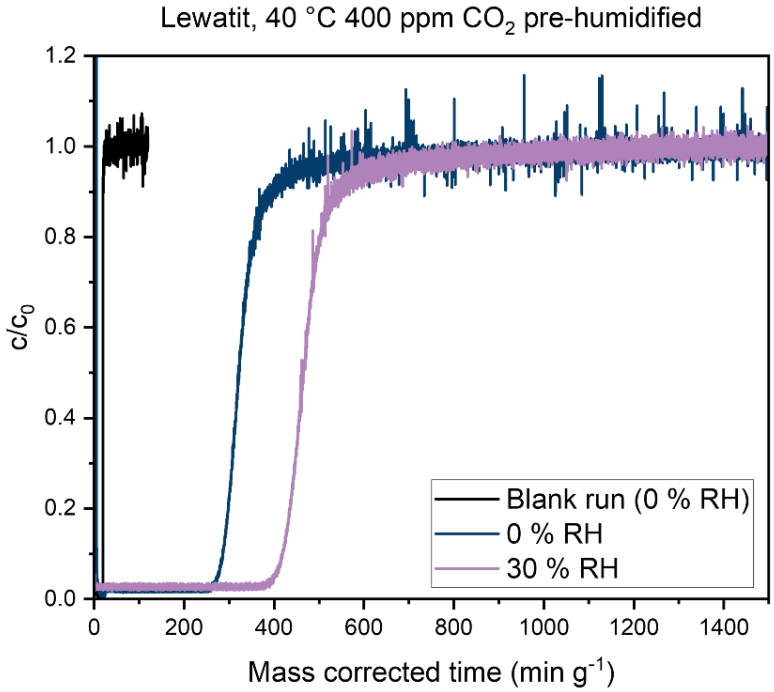

Figure 37: Lewatit VP OC 1065 CO_2 breakthrough curves (BTC) at 40 ºC.

The co-adsorption data (Table 6) offer more nuanced comprehension of the interaction between H_2O and CO_2 uptake on both Lewatit and PEI-CNFs under varying humidity and temperature conditions, building on the insights obtained from the breakthrough curves analysis. The samples were initially pre-saturated with water vapor at the designated relative humidity (RH), afterwards, CO_2 was introduced. The data show that 33 wt% PEI-CNFs increased H_2O uptake with relative humidity, reaching 9.88 mmol g^{-1} at 25 ºC and 70 % RH. CO_2 uptake also increased with humidity, reaching 1.581 mmol g^{-1} at 70 % RH. At 40 ºC and 30 % RH, H_2O slightly decreased, but CO_2 uptake remained high.

This suggests that the presence of moisture enhances CO_2 capture, probably through facilitated adsorption mechanisms involving H_2O.

For Lewatit, H_2O uptake is generally lower across all conditions compared to PEI-CNFs. At 25 °C and 70 % RH, Lewatit absorbs 3.101 mmol g^{-1} of H_2O, which is roughly one-third that of PEI-CNFs at the same conditions. CO_2 uptake also increases with humidity but remains significantly lower than PEI-CNFs, reaching only 0.876 mmol g^{-1} at 70 % RH and 25 °C. At 40 °C, both H_2O and CO_2 uptake decrease noticeably to 0.654 mmol g^{-1} and 0.424 mmol g^{-1}, respectively, at 30 % RH, showing a stronger negative effect of temperature on Lewatit's adsorption capacities compared to PEI-CNFs.

Table 6: Co-adsorption of H_2O and CO_2 on 33 wt% PEI-CNFs and Lewatit under different temperatures and relative humidities.

Conditions	Lewatit VP OC 1065		33 wt% PEI-CNFs	
	H_2O (mmol g^{-1})	CO_2 (mmol g^{-1})	H_2O (mmol g^{-1})	CO_2 (mmol g^{-1})
25 °C, 0 % RH	-	0.535	-	0.62
25 °C, 30 % RH	1.43	0.724	3.743	1.421
25 °C, 70 % RH	3.101	0.876	9.888	1.581
40 °C, 0 % RH	-	0.272	-	0.846
40 °C, 30 % RH	0.654	0.424	3.097	1.394

Overall, the data reveal that PEI-CNFs exhibit superior co-adsorption capacities for both H_2O and CO_2 relative to Lewatit, with moisture playing a significant role in increasing CO_2 uptake. Increasing RH enhances H_2O adsorption significantly, which in turn increases CO_2 adsorption. The weak performance of Lewatit, particularly at elevated temperatures, suggests it is less effective for CO_2 capture in humid or warm environments. This co-adsorption behavior highlights the importance of considering H_2O vapor effects and material choice in designing sorbents for efficient CO_2 capture under realistic conditions.

This chapter presented a comprehensive evaluation of the structural, textural, and adsorption characteristics of CNF subjected to various treatments aimed at enhancing their performance for DAC of CO_2. The U_CNF and O_CNF samples exhibited nearly flat pore size distributions with very low microporosity and BET surface area of approximately 7.8 and 77.6 m^2 g^{-1} respectively. This oxidative treatment primarily introduced oxygen-containing functional groups, confirmed by the TGA results, enhancing the material's reactivity without significantly increasing porosity. The introduction of KOH chemical activation dramatically altered the CNF texture, creating extensive microposity, as reflected by a large increase in BET surface area from 7.0 m^2 g^{-1} for U_CNFs to over 436.9 m^2 g^{-1} for the A_CNF sample, and pore volume rising from 0.014 cm^3 g^{-1} to 0.239 cm^3 g^{-1}. The pore size distribution shifted to feature a dominant peak below 2 nm, consistent with robust micropore formation.

The APTMS grafting, which introduces primary amine groups, represented a pivotal step for functional enhancement. The AOS_2 sample, functionalized via APTMS grafting for 20 h, achieved the highest CO_2 uptake among all samples, demonstrating an increase in CO_2

adsorption capacity compared to the U_CNF in the same conditions. This gain is attributable to the strong chemisorptive interaction between CO_2 molecules and the primary amines, facilitating carbamate formation under low-pressure conditions. Pore size analysis revealed that aminosilane grafting moderately reduced BET surface area to approximately 58.9 m^2 g^{-1} but preserved sufficient pore accessibility, as the broad mesoporous peak around 3-4 nm remained prominent.

Comparative BTC measurements on Lewatit and 33 wt% PEI-CNFs showed improved dynamic CO_2 capacity for amine-functionalized adsrobents, especially under humid conditions. The BTC data for the AOS_2 sample is unfortunately unavailable. The PEI-CNFs showed significantly enhanced CO_2 retention times and capacities, demonstrating the important role of amine groups in facilitating CO_2 adsorption. Humidity further improves adsorption performance by promoting co-adsorption synergy between H_2O and CO_2, as reflected in both breakthrough curves and co-adsorption data.

This dynamic behavior, paired with the hierarchical pore structure and chemical accessibility afforded by silanization in AOS_2, suggests that similar enhanced CO_2 capture performance can be expected for AOS_2 in DAC-relevant humid environments. Overall, the combined pore architecture and amine functionality represent a promising strategy to maximize dynamic adsorption efficiency while maintaining resilience in real-world, moist air conditions.

The findings from this chapter demonstrate that KOH activation effectively develops microporosity essential for physisorption while aminosilane grafting imparts the necessary chemisorptive functionality to selectively capture CO_2 at low concentrations. This dual modification strategy is key for optimizing CNFs to balance pore accessibility and chemical reactivity, setting the stage for their use in DAC technologies.

GENERAL CONCLUSION AND PERSPECTIVES

GENERAL CONCLUSION

This thesis has systematically explored the design, synthesis, characterization, and performance evaluation of carbon nanofiber (CNF)-based adsorbents tailored for direct air capture (DAC) of CO_2. Through advanced methods including KOH chemical activation, oxidation, and aminosilane grafting with (3-aminopropyl)trimethoxysilane (APTMS), the study established how synergistic modification of pore structure and surface chemistry drives adsorption efficacy under ultradilute CO_2 conditions.

The findings confirmed that a balance between microporosity and chemical functionality is essential for effective CO_2 uptake. While pristine and oxidized showed limited physisorption capacity under DAC-relevant pressures due to their restricted porosity, chemical activation successfully enhanced surface area and pore accessibility. Nonetheless, these improvements alone were insufficient to achieve the necessary adsorption selectivity, highlighting the critical role of amine groups. Functionalization with APTMS introduced primary amines that provided strong chemisorptive sites, enabling superior performance compared to non-functionaized materials.

The combined structural and surface modification established in this work underline the potential of CNF-based adsorbents as a versatile platform for DAC applications. Their high tunability offers promising prospects for reducing the energy penalty associated with capture processes and improving the overall efficiency of DAC systems. However, further progress depends on the development of scalable cost-efficient synthesis strategies and ensuring the long-term oxidative and thermal stability of amine-functionalized CNFs.

Perspectives

Future research should focus on optimizing amine loading and distribution through controlled grafting techniques to enhance functional group density while maintaining pore accessibility. Additionally, thorough investigations of stability and regeneration under actual humid and oxidative DAC environments are needed to test long-term durability and performance preservation. For practical use, it will be very important to work on making scalable manufacturing processes and adding these materials to modular DAC systems. Last but not least, full life cycle evaluations and technico-economic studies are needed to compare CNF-based sorbents to existing DAC technologies and to help them become commercially viable. These strategic actions will be important for making these materials more useful in efficient carbon capture technologies and helping the world meet its climate objectives.

REFERENCES

Aguilar-Ccuno, C., Churata, R., Martínez, K., & Almirón, J. (2025). Development and Characterization of KOH-Activated Carbons Derived from Zeolite-Catalyzed Pyrolysis of Waste Tires. *Sustainability (Switzerland)*, *17*(11), 4822. https://doi.org/10.3390/SU17114822/S1

Bao, S., Zheng, X., Xu, Z., Ji, B., Yang, Z., Sun, W., Guo, L., Zhu, Y., Mei, J., Rong, J., & Li, Z. (2025). Advancements in the development of porous nanomaterials for CO2 capture of deep decarbonization: Pore structure and chemical group optimization. *Journal of Environmental Chemical Engineering*, *13*(1), 115171. https://doi.org/10.1016/J.JECE.2024.115171

Carneiro, J. S. A., Innocenti, G., Moon, H. J., Guta, Y., Proaño, L., Sievers, C., Sakwa-Novak, M. A., Ping, E. W., & Jones, C. W. (2023). Insights into the Oxidative Degradation Mechanism of Solid Amine Sorbents for CO_2 Capture from Air: Roles of Atmospheric Water. *Angewandte Chemie*, *135*(24), e202302887. https://doi.org/10.1002/ANGE.202302887

Chang, S. S., Clair, B., Ruelle, J., Beauchêne, J., Di Renzo, F., Quignard, F., Zhao, G. J., Yamamoto, H., & Gril, J. (2009). Mesoporosity as a new parameter for understanding tension stress generation in trees. *Journal of Experimental Botany*, *60*(11), 3023–3030. https://doi.org/10.1093/JXB/ERP133

Chiang, Y.-C., Huang, C.-C., Chin, W.-T., Hsieh, W.-H., Sheu, J.-S., & Ragulskis, M. (2021). Carbon Dioxide Adsorption on Carbon Nanofibers with Different Porous Structures. *Applied Sciences 2021, Vol. 11, Page 7724*, *11*(16), 7724. https://doi.org/10.3390/APP11167724

Choi, S., Drese, J. H., & Jones, C. W. (2009). Adsorbent Materials for Carbon Dioxide Capture from Large Anthropogenic Point Sources. *ChemSusChem*, *2*(9), 796–854. https://doi.org/10.1002/CSSC.200900036

de Falco, G., Florent, M., Jagiello, J., Cheng, Y., Daemen, L. L., Ramirez-Cuesta, A. J., & Bandosz, T. J. (2021). Alternative view of oxygen reduction on porous carbon electrocatalysts: the substance of complex oxygen-surface interactions. *IScience*, *24*(3), 102216. https://doi.org/10.1016/J.ISCI.2021.102216

Fischer, T., Kretzschmar, A., Selmert, V., Jovanovic, S., Kungl, H., Tempel, H., & Eichel, R.-A. (2024). *Post-treatment strategies for pyrophoric KOH-activated carbon nanofibres †*. https://doi.org/10.1039/d3ra07096d

Fu, Y. (n.d.). *Experimental Study of Different Sorbents for Direct Air Capture*.

Fuss, S., Lamb, W. F., Callaghan, M. W., Hilaire, J., Creutzig, F., Amann, T., Beringer, T., De Oliveira Garcia, W., Hartmann, J., Khanna, T., Luderer, G., Nemet, G. F., Rogelj, J., Smith, P., Vicente, J. V., Wilcox, J., Del Mar Zamora Dominguez, M., & Minx, J. C. (2018). Negative emissions - Part 2: Costs, potentials and side effects. *Environmental Research Letters*, *13*(6). https://doi.org/10.1088/1748-9326/AABF9F

Gao, Y., Yue, Q., Gao, B., & Li, A. (2020). Insight into activated carbon from different kinds of chemical activating agents: A review. *Science of The Total Environment*, *746*, 141094. https://doi.org/10.1016/J.SCITOTENV.2020.141094

Gebald, C. (2014). *Development of amine-functionalized adsorbent for carbon dioxide capture from atmospheric air*. https://doi.org/10.3929/ETHZ-A-010171623

Gunawardene, O. H. P., Gunathilake, C. A., Vikrant, K., & Amaraweera, S. M. (2022). Carbon Dioxide Capture through Physical and Chemical Adsorption Using Porous Carbon Materials: A Review. *Atmosphere 2022, Vol. 13, Page 397*, *13*(3), 397. https://doi.org/10.3390/ATMOS13030397

Guo, Z., Wu, N., Wu, Y., Sun, C., Wu, H., & Li, Q. (2022). Anion-induced morphology control of Al-fumarate MOFs via synergetic coordination and hydrogen bond effects for graded dehumidification. *Microporous and Mesoporous Materials*, *343*, 112168. https://doi.org/10.1016/J.MICROMESO.2022.112168

Hack, J., Maeda, N., & Meier, D. M. (2022). Review on CO_2 Capture Using Amine-Functionalized Materials. *ACS Omega*, *7*(44), 39520–39530. https://doi.org/10.1021/ACSOMEGA.2C03385/ASSET/IMAGES/LARGE/AO2C03385_0004.JPEG

Han, Y., Li, R., Brückner, C., & Vadas, T. M. (2018). Controlling the Surface Oxygen Groups of Polyacrylonitrile-Based Carbon Nanofiber Membranes While Limiting Fiber Degradation. *C*, *4*(3), 40. https://doi.org/10.3390/C4030040

Hansen, J., Sato, M., & Kharecha, P. (n.d.). *Earth's Energy Imbalance and Implications*.

Heydari-Gorji, A., Belmabkhout, Y., & Sayari, A. (2011). Polyethylenimine-impregnated mesoporous silica: Effect of amine loading and surface alkyl chains on CO_2 adsorption. *Langmuir*, *27*(20), 12411–12416. https://doi.org/10.1021/LA202972T/SUPPL_FILE/LA202972T_SI_001.PDF

Kundu, S., Khandaker, T., Anik, M. A. A. M., Hasan, M. K., Dhar, P. K., Dutta, S. K., Latif, M. A., & Hossain, M. S. (2024). A comprehensive review of enhanced CO_2 capture using activated carbon derived from biomass feedstock. *RSC Advances*, *14*(40), 29693–29736. https://doi.org/10.1039/D4RA04537H

Liang, S., Li, G., & Tian, R. (2016). Multi-walled carbon nanotubes functionalized with a ultrahigh fraction of carboxyl and hydroxyl groups by ultrasound-assisted oxidation. *Journal of Materials Science*, *51*(7), 3513–3524. https://doi.org/10.1007/S10853-015-9671-Z

Lim, Y., Park, H., Walsh, A., & Kim, J. (2025). Accelerating CO_2 direct air capture screening for metal-organic frameworks with a transferable machine learning force field. *Matter*. https://doi.org/10.1016/j.matt.2025.102203

Liu, P., Sun, S., Huang, S., Wu, Y., Li, X., Wei, X., & Wu, S. (2024). KOH Activation Mechanism in the Preparation of Brewer's Spent Grain-Based Activated Carbons. *Catalysts 2024, Vol. 14, Page 814*, *14*(11), 814. https://doi.org/10.3390/CATAL14110814

Low, M. Y. A., Danaci, D., Azzan, H., Woodward, R. T., & Petit, C. (2023). Measurement of Physicochemical Properties and CO_2, N_2, Ar, O_2, and H_2O Unary Adsorption Isotherms of Purolite A110 and Lewatit VP OC 1065 for Application in Direct Air Capture. *Journal of Chemical and Engineering Data*, *68*(12), 3499–3511. https://doi.org/10.1021/ACS.JCED.3C00401/SUPPL_FILE/JE3C00401_SI_003.ZIP

Lundstedt, C. (2019). *BET Theory and how its used to calculate surface area HORIBA Scientific Particle Analysis*.

Maruccia, E., Ferrari, S., Bartoli, M., Lucherini, L., Meligrana, G., Pirri, C. F., Saracco, G., & Gerbaldi, C. (2021). Effect of thermal stabilization on pan-derived electrospun carbon nanofibers for co2 capture. *Polymers*, *13*(23). https://doi.org/10.3390/POLYM13234197,

McQueen, N., Gomes, K. V., McCormick, C., Blumanthal, K., Pisciotta, M., & Wilcox, J. (2021). A review of direct air capture (DAC): scaling up commercial technologies and innovating for the future. *Progress in Energy*, *3*(3), 032001. https://doi.org/10.1088/2516-1083/ABF1CE

Moosavi, S., Wei Lai, C., Gan, S., Zamiri, G., Akbarzadeh Pivehzhani, O., & Rafie Johan, M. (2020). *Application of Efficient Magnetic Particles and Activated Carbon for Dye Removal from Wastewater*. https://doi.org/10.1021/acsomega.0c01905

Nandi, R., Jha, M. K., Guchhait, S. K., Sutradhar, D., & Yadav, S. (2023). Impact of KOH Activation on Rice Husk Derived Porous Activated Carbon for Carbon Capture at Flue Gas alike Temperatures with High CO2/N2 Selectivity. *ACS Omega*, *8*(5), 4802–4812. https://doi.org/10.1021/ACSOMEGA.2C06955/ASSET/IMAGES/LARGE/AO2C06955_0012.JPEG

Othman, F. E. C., Yusof, N., Ismail, A. F., Rushdan, A. I., & Low, H. Y. (2024). Electrospun graphene carbon nanofibers for CO2 capture and storage: A review. *Journal of Environmental Chemical Engineering*, *12*(2), 112014. https://doi.org/10.1016/J.JECE.2024.112014

Petrovic, B., Gorbounov, M., & Masoudi Soltani, S. (2021). Influence of surface modification on selective CO2 adsorption: A technical review on mechanisms and methods. *Microporous and Mesoporous Materials*, *312*, 110751. https://doi.org/10.1016/J.MICROMESO.2020.110751

Pohlkemper, F., Rolfes, S., Bouhrara, M., Röding, T., & Gries, T. (2024). Market analysis of carbon fiber production with reference to the oxidation ovens used. *Applied Research*, *3*(4). https://doi.org/10.1002/APPL.202200119

Raganati, F., Miccio, F., & Ammendola, P. (2021). Adsorption of Carbon Dioxide for Post-combustion Capture: A Review. *Energy and Fuels*, *35*(16), 12845–12868. https://doi.org/10.1021/ACS.ENERGYFUELS.1C01618/ASSET/IMAGES/LARGE/EF1C01618_0004.JPEG

Samanta, A., Zhao, A., Shimizu, G. K. H., Sarkar, P., & Gupta, R. (2012). Post-combustion CO 2 capture using solid sorbents: A review. *Industrial and Engineering Chemistry Research*, *51*(4), 1438–1463. https://doi.org/10.1021/IE200686Q/ASSET/IMAGES/LARGE/IE-2011-00686Q_0013.JPEG

Sanz-Pérez, E. S., Murdock, C. R., Didas, S. A., & Jones, C. W. (2016). Direct Capture of CO_2 from Ambient Air. *Chemical Reviews*, *116*(19), 11840–11876. https://doi.org/10.1021/ACS.CHEMREV.6B00173/ASSET/IMAGES/LARGE/CR-2016-00173P_0028.JPEG

Sekizkardes, A. K., Wang, P., Hoffman, J., Budhathoki, S., & Hopkinson, D. (2022). Amine-functionalized porous organic polymers for carbon dioxide capture. *Materials Advances*, *3*(17), 6668–6686. https://doi.org/10.1039/D2MA00235C

Sharma, G. K., James, N. R., Sharma, G. K., & James, N. R. (2022). Electrospinning: The Technique and Applications. *Recent Developments in Nanofibers Research*. https://doi.org/10.5772/INTECHOPEN.105804

Shi, X., Xiao, H., Azarabadi, H., Song, J., Wu, X., Chen, X., & Lackner, K. S. (2020). Sorbents for the Direct Capture of CO_2 from Ambient Air. *Angewandte Chemie - International Edition*, *59*(18), 6984–7006. https://doi.org/10.1002/ANIE.201906756;SUBPAGE:STRING:FULL

Sim, Y. T., & Ruhaimi, A. H. (2022). *Recent progress on (3-Aminopropyl)triethoxysilane (APTES) functionalized-adsorbent for CO_2 capture*. 12008. https://doi.org/10.1088/1742-6596/2259/1/012008

Siriwardane, R. V., Shen, M. S., Fisher, E. P., & Poston, J. A. (2001). Adsorption of CO_2 on molecular sieves and activated carbon. *Energy and Fuels*, *15*(2), 279–284. https://doi.org/10.1021/EF000241S/ASSET/IMAGES/LARGE/EF000241SF00012.JPEG

Sodiq, A., Abdullatif, Y., Aissa, B., Ostovar, A., Nassar, N., El-Naas, M., & Amhamed, A. (2023). A review on progress made in direct air capture of CO_2. *Environmental Technology & Innovation*, *29*, 102991. https://doi.org/10.1016/J.ETI.2022.102991

Suba, M., Verdeș, O., Borcănescu, S., & Popa, A. (2024). Effect of Temperature on CO_2 Adsorption onto Amine-Functionalized KIT-6 Adsorbents. *Molecules 2024, Vol. 29, Page 3172*, *29*(13), 3172. https://doi.org/10.3390/MOLECULES29133172

Suresh, K., Reddy, K., Varghese, A. M., Ogungbenro, A. E., & Karanikolos, G. N. (2023). Aminosilane-Modified Ordered Hierarchical Nanostructured Silica for Highly-Selective Carbon Dioxide Capture at Low Pressure. *ACS Applied Engineering Materials*, *1*(2), 720–733. https://doi.org/10.1021/ACSAENM.2C00136

The Ideal Gas Law. (n.d.). Retrieved September 8, 2025, from https://www.engineeringtoolbox.com/ideal-gas-law-d_157.html

Thommes, M., Kaneko, K., Neimark, A. V., Olivier, J. P., Rodriguez-Reinoso, F., Rouquerol, J., & Sing, K. S. W. (2015a). Physisorption of gases, with special reference to the evaluation of surface area and pore size distribution (IUPAC Technical Report). *Pure and Applied Chemistry*, *87*(9–10), 1051–1069. https://doi.org/10.1515/PAC-2014-1117/ASSET/GRAPHIC/J_PAC-2014-1117_FIG_010.JPG

Thommes, M., Kaneko, K., Neimark, A. V., Olivier, J. P., Rodriguez-Reinoso, F., Rouquerol, J., & Sing, K. S. W. (2015b). Physisorption of gases, with special reference to the

evaluation of surface area and pore size distribution (IUPAC Technical Report). *Pure and Applied Chemistry*, *87*(9–10), 1051–1069. https://doi.org/10.1515/PAC-2014-1117

Thommes, M., Kaneko, K., Neimark, A. V., Olivier, J. P., Rodriguez-Reinoso, F., Rouquerol, J., & Sing, K. S. W. (2015c). Physisorption of gases, with special reference to the evaluation of surface area and pore size distribution (IUPAC Technical Report). *Pure and Applied Chemistry*, *87*(9–10), 1051–1069. https://doi.org/10.1515/PAC-2014-1117/ASSET/GRAPHIC/J_PAC-2014-1117_FIG_010.JPG

Veneman, R., Frigka, N., Zhao, W., Li, Z., Kersten, S., & Brilman, W. (2015). Adsorption of H_2O and CO_2 on supported amine sorbents. *International Journal of Greenhouse Gas Control*, *41*, 268–275. https://doi.org/10.1016/j.ijggc.2015.07.014

Wang, B., Li, S., & Tan, W. (2021). Preparation of Flax Residue Activated Carbon by KOH Method and Its Electrode Performance. *Materials Sciences and Applications*, *12*(09), 417–435. https://doi.org/10.4236/MSA.2021.129028

Weltgrößte DAC-Anlage geht in Island in Betrieb | SOLARIFY. (n.d.). Retrieved July 17, 2025, from https://www.solarify.eu/2021/09/12/101-weltgroesste-dac-anlage-geht-in-island-ins-betrieb/

Williams, N. E., Oba, O. A., & Aydinlik, N. P. (2022). Modification, Production, and Methods of KOH-Activated Carbon. *ChemBioEng Reviews*, *9*(2), 164–189. https://doi.org/10.1002/CBEN.202100030;CTYPE:STRING:JOURNAL

Yagmur Goren, A., Erdemir, D., & Dincer, I. (2024). Comprehensive review and assessment of carbon capturing methods and technologies: An environmental research. In *Environmental Research* (Vol. 240). https://doi.org/10.1016/j.envres.2023.117503

Yao, S., Li, C., Jackson, M., & Strachan, A. (2024). Molecular Modeling of Stabilization during Processing of Polyacrylonitrile-Based Carbon Fibers. *Macromolecules*, *57*(12), 5578–5588. https://doi.org/10.1021/ACS.MACROMOL.3C02487/ASSET/IMAGES/LARGE/MA3C02487_0014.JPEG

Young, J., García-Díez, E., Garcia, S., & Van Der Spek, M. (2021). The impact of binary water–CO_2 isotherm models on the optimal performance of sorbent-based direct air capture processes. *Energy & Environmental Science*, *14*(10), 5377–5394. https://doi.org/10.1039/D1EE01272J

Yue, Z. R., Jiang, W., Wang, L., Gardner, S. D., & Pittman, C. U. (1999). Surface characterization of electrochemically oxidized carbon fibers. *Carbon*, *37*(11), 1785–1796. https://doi.org/10.1016/S0008-6223(99)00047-0

Zentou, H., Hoque, B., Abdalla, M. A., Saber, A. F., Abdelaziz, O. Y., Aliyu, M., Alkhedhair, A. M., Alabduly, A. J., & Abdelnaby, M. M. (2025). Recent advances and challenges in solid sorbents for CO_2 capture. *Carbon Capture Science & Technology*, *15*, 100386. https://doi.org/10.1016/J.CCST.2025.100386

Zhang, X. G., Buthiyappan, A., Jewaratnam, J., Metselaar, H. S. C., & Raman, A. A. A. (2024). Bifunctional materials for integrated CO2 capture and conversion: review on adsorbent

and catalyst types, recent advances, and challenges. *Journal of Environmental Chemical Engineering*, *12*(1). https://doi.org/10.1016/J.JECE.2023.111799

Zhao, M., Huang, L., Gao, Y., Wang, Z., Liang, S., Zhu, X., Wang, Q., He, H., & O'Hare, D. (2025). Design of Ultra-Stable Solid Amine Adsorbents and Mechanisms of Hydroxyl Group-Dependent Deactivation for Reversible CO2 Capture from Flue Gas. *Nano-Micro Letters*, *17*(1), 1–19. https://doi.org/10.1007/S40820-025-01664-W/FIGURES/2

Zhao, S., Zhang, Y., Li, L., Feng, J., Qiu, W., Ning, Y., Huang, Z., & Lin, H. (2025). Degradation of amine-functionalized adsorbents in carbon capture and direct air capture applications: Mechanism and solutions. *Separation and Purification Technology*, *354*, 129586. https://doi.org/10.1016/J.SEPPUR.2024.129586

ANNEX

EDX results

1- AOS-2

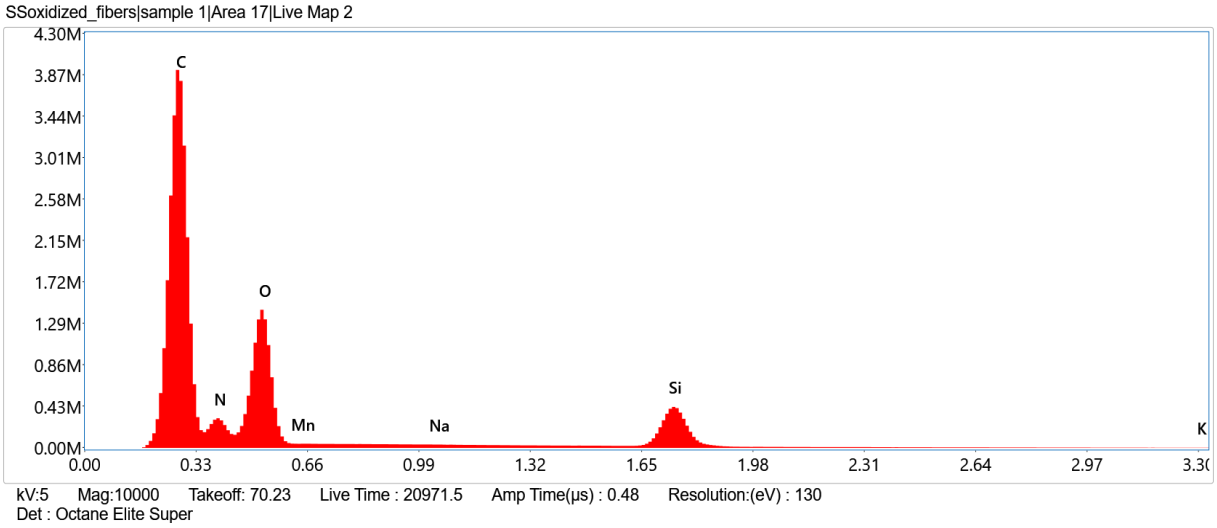

eZAF Quant Result - Analysis Uncertainty: 7.83 %

Element	Weight %	MDL	Atomic %	Error %	Net Int.	R	A	F
C K	72.4	0.01	79.3	4.8	1196.3	0.9476	0.7499	1.0000
N K	5.3	0.01	5.0	0.5	86.6	0.9531	0.4216	1.0000
O K	15.1	0.01	12.4	0.9	436.8	0.9576	0.6125	1.0000
Na K	0.0	0.01	0.0	0.0	0.6	0.9690	0.8993	1.0029
Si K	7.1	0.01	3.3	0.2	167.4	0.9792	0.9790	1.0040
K K	0.0	0.00	0.0	0.0	0.0	0.9946	0.9974	1.0232
Mn L	0.0	0.00	0.0	0.0	0.0	0.9605	0.6752	1.0000

2- UOS_1

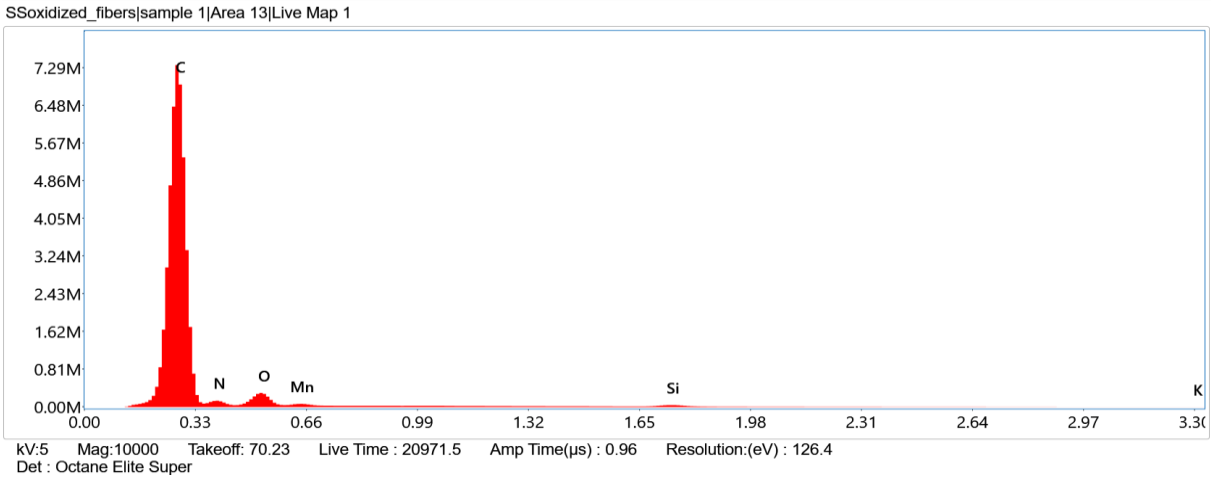

eZAF Quant Result - Analysis Uncertainty: 6.00 %

Element	Weight %	MDL	Atomic %	Error %	Net Int.	R	A	F
C K	95.4	0	96.7	4.9	2071.3	0.9534	0.8533	1.0000
N K	1.5	0.01	1.3	0.1	24.1	0.9584	0.3644	1.0000
O K	2.3	0.01	1.7	0.1	71.1	0.9625	0.5777	1.0000
Si K	0.5	0	0.2	0.0	12.6	0.9820	0.9822	1.0056
K K	0.1	0.03	0.0	0.0	0.3	0.9954	0.9918	1.0320
Mn L	0.3	0.01	0.1	0.0	4.4	0.9651	0.7009	1.0000

3- UOS_2

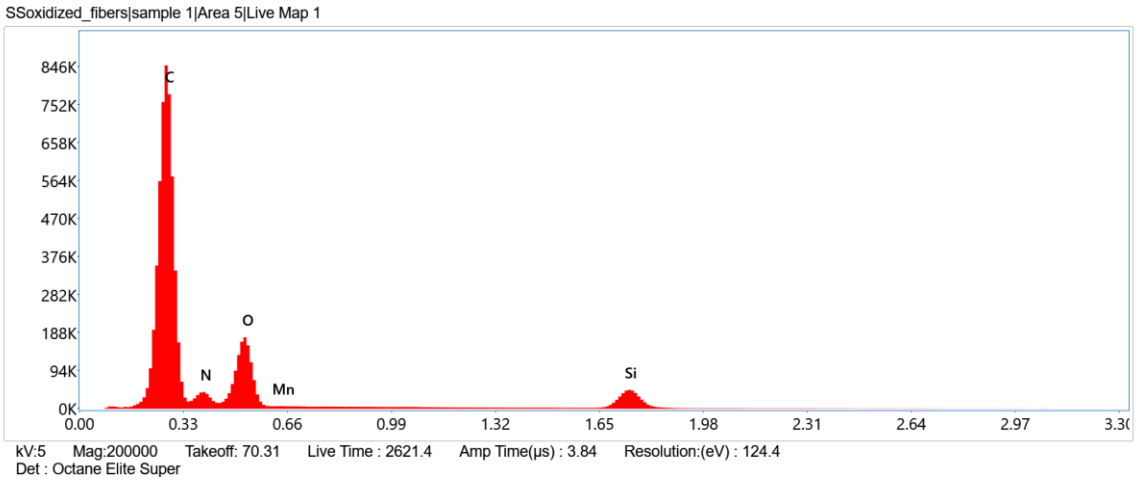

eZAF Quant Result - Analysis Uncertainty: 6.57 %

Element	Weight %	MDL	Atomic %	Error %	Net Int.	R	A	F
C K	80.7	0.01	85.7	4.9	1849.1	0.9499	0.7888	1.0000
N K	4.3	0.02	3.9	0.4	87.2	0.9553	0.4007	1.0000
O K	10.5	0.01	8.4	0.7	391.6	0.9595	0.5995	1.0000
Si K	4.4	0.01	2.0	0.1	138.3	0.9803	0.9802	1.0044
Mn L	0.1	0.02	0.0	0.0	0.9	0.9623	0.6843	1.0000

4- UOS_3

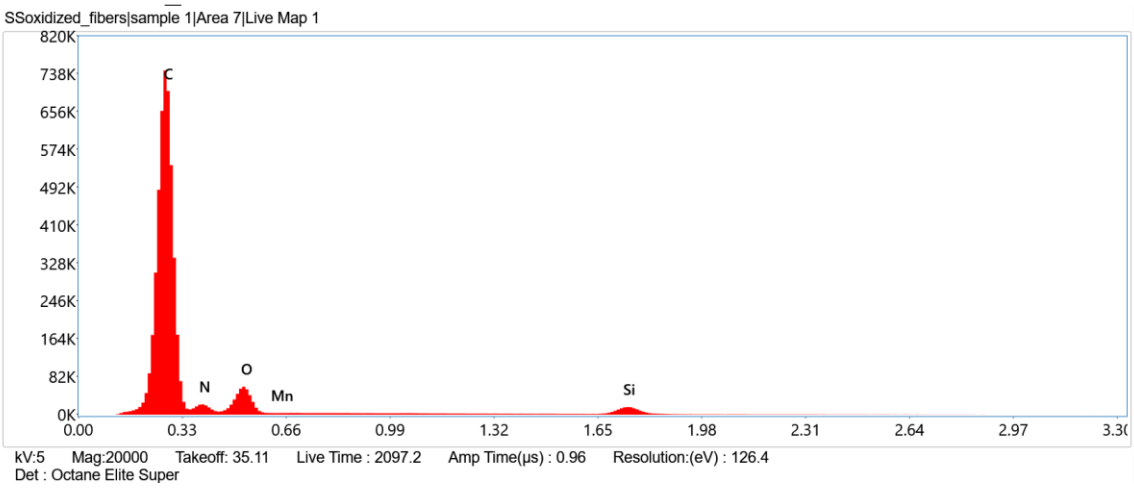

eZAF Quant Result - Analysis Uncertainty: 5.74 %

Element	Weight %	MDL	Atomic %	Error %	Net Int.	R	A	F
C K	90.7	0.01	93.2	5.0	2101.3	0.9524	0.8301	1.0000
N K	2.8	0.02	2.5	0.3	51.4	0.9576	0.3764	1.0000
O K	4.6	0.01	3.5	0.3	159.5	0.9617	0.5840	1.0000
Si K	2.0	0.01	0.9	0.1	59.3	0.9815	0.9818	1.0051
Mn L	0.0	0.00	0.0	0.0	0.0	0.9643	0.6966	1.0000